








## Article

# Metabolic Dynamics of Primary Reserves During Germination and Early Growth of Cultivated Brazil Nut Tree Genotypes

Elmer Gonçalves <sup>1,2</sup> , Josiane Carvalho <sup>1,\*</sup> , Caris Viana <sup>1</sup>, Pedro Santos <sup>1,2</sup> , Katharine Gonçalves <sup>1,3</sup> , Karen Costa <sup>4</sup>, Auxiliadora Martins <sup>5</sup>, Silvana Silva <sup>6</sup>, Roberval Lima <sup>7</sup> , Patrícia Albuquerque <sup>6</sup>, Andreia Fernandes <sup>1</sup>, Wagner Araújo <sup>5</sup>  and José Francisco Gonçalves <sup>1,\*</sup> 

<sup>1</sup> Laboratory of Plant Physiology and Biochemistry, National Institute of Amazonian Research, Ministry of Science, Technology, and Innovation, Manaus 69060-062, AM, Brazil; elmer050995@gmail.com (E.G.); carisviana@hotmail.com (C.V.); santosp@gmail.com (P.S.); katharineduardedg@gmail.com (K.G.); varmes@inpa.gov.br (A.F.)

<sup>2</sup> Bionorte Post Graduate Program (BIONORTE), University of the State of Amazonas, Boca do Acre 69065-001, AM, Brazil

<sup>3</sup> Post Graduate Program in Biochemistry (PGP-Biochemistry), Federal University of Ceará (FUC), Fortaleza 60020-181, CE, Brazil

<sup>4</sup> Faculty of Agronomy, Institute of Studies in Agrarian and Regional Development—ISARD, Federal University of Southern and Southeastern Pará (FUSPP), Marabá 68500-000, PA, Brazil; karencosta@unifesspa.edu.br

<sup>5</sup> National Institute of Science and Technology on Plant Physiology Under Stress Conditions, Department of Plant Biology, Federal University of Viçosa, Viçosa 36570-900, MG, Brazil; auxiliamartins82@gmail.com (A.M.); wlaraujo@ufv.br (W.A.)

<sup>6</sup> School of Technology, Amazonas State University—ASU, Manaus 69050-020, AM, Brazil; silvana\_nasc@hotmail.com (S.S.); patialbuq@hotmail.com (P.A.)

<sup>7</sup> Embrapa Western Amazon, Manaus 69010-970, AM, Brazil; roberval.lima@embrapa.br

\* Correspondence: josiane.celerino@gmail.com (J.C.); jfc@inpa.gov.br (J.F.G.)

## Abstract

Given the reduced resilience of the Amazon rainforest due to deforestation, identifying high-quality genetic markers for the propagation of native species is crucial for forest regeneration. This study investigated metabolic dynamics during Brazil nut (*Bertholletia excelsa*) germination to identify biochemical markers for selecting superior genotypes. We analyzed primary reserves (carbohydrates, lipids, proteins) and minerals in two genotypes, 606 and Santa Fé, in seven germination stages. Our results revealed distinct metabolic patterns. Genotype 606 showed 101.73% greater efficiency in the transient accumulation of starch, 34.86% higher degradation of lipids, and 34.86% higher transitory synthesis of soluble proteins. Conversely, Santa Fé was 16.8% more efficient in amino acid synthesis and 795.33% in boron compartmentalization, though less so in sucrose (2.17%) and in lipid synthesis (24.84%). Overall, early germination stages involved starch, sucrose degradation and mineral consumption. During post-germinative stages, protein and lipid degradation likely fueled gluconeogenic pathways and supported carbohydrate synthesis and seedling growth. This work increases the knowledge on Brazil nut germination physiology and identifies metabolic markers that differentiate genotypes. These findings are fundamental for our understanding of primary metabolism turnover in *B. excelsa* and provide a basis to support forest restoration and genetic improvement programs. In addition, we hope to contribute to the selection of superior high-performance genotypes, which are essential for recovering degraded areas and enhancing productive plantations in the Amazon region.

**Keywords:** metabolic turnover; germination physiology; *Bertholletia excelsa* Bonpl.; seed biochemistry; metabolic markers; primary metabolism



Academic Editor: Božena Šerá

Received: 4 September 2025

Revised: 5 November 2025

Accepted: 13 November 2025

Published: 17 November 2025

**Citation:** Gonçalves, E.; Carvalho, J.; Viana, C.; Santos, P.; Gonçalves, K.; Costa, K.; Martins, A.; Silva, S.; Lima, R.; Albuquerque, P.; et al. Metabolic Dynamics of Primary Reserves During Germination and Early Growth of Cultivated Brazil Nut Tree Genotypes. *Seeds* **2025**, *4*, 60. <https://doi.org/10.3390/seeds4040060>

**Copyright:** © 2025 by the authors. Licensee MDPI, Basel, Switzerland. This article is an open access article distributed under the terms and conditions of the Creative Commons Attribution (CC BY) license (<https://creativecommons.org/licenses/by/4.0/>).

## 1. Introduction

Indiscriminate deforestation has diminished the resilience of the Amazon rainforest, leading to many negative impacts, such as rising temperatures, extreme droughts, and an increased incidence of wildfires, among others [1]. In this context, research focused on forest regeneration using seeds from native Amazonian species must be encouraged [2–5].

Thus, understanding the factors and processes involved in the germination of these seeds is of vital importance, as it enables the selection of quality markers related to seedling propagation. Among these factors, the plant's genetic makeup is directly associated with its seed reserve content (carbohydrates, lipids, proteins, and minerals) and how these are metabolized, even among different individuals of the same species [6–8]. These intraspecific differences can be attributed to inherent genotypic characteristics and, therefore, can be used as markers of these genotypes.

Among the native Amazonian forest species with potential for restoring degraded areas, the Brazil nut tree (*Bertholletia excelsa* Bonpl) (Lecythidaceae) stands out due to its high plasticity, resilience, and accumulation of biomass [9–14]. These characteristics make it a target for genetic improvement initiatives. One of the most effective of these is located at Fazenda Aruanã, in Itacoatiara, Amazonas, Brazil, which hosts the world's largest plantation of Brazil nut trees for the restoration of degraded areas [14].

At Fazenda Aruanã, there are grafted genotypes, approximately 40 years old, named Manoel Pedro, Santa Fé, Aruanã, 606 and 609. These genotypes differ in the morphological, productive and ecophysiological aspects of the adult plants [10,15]. Of these genotypes, Manoel Pedro exhibits the best characteristics, while 606 shows inferior responses, and Santa Fé is in an intermediate position. However, different outcomes are observed in the germination parameters of two of these genotypes (606 and Santa Fé), in which the genotype 606 has a higher germination rate and germination speed index [10]. Furthermore, Gonçalves et al. (2024) [10] observed distinct patterns between seed morphology and germination in these two genotypes.

Regarding the morphophysiological characteristics of *B. excelsa* seeds, they are bitegmic, consisting of a woody testa and tegmen, which impose physical dormancy. They are also considered recalcitrant [10]. Moreover, it is suggested that they also exhibit physiological dormancy due to embryo immaturity immediately after fruit fall [16].

Concerning the embryo of the species, there is no morphological differentiation [10], and its reserve composition is predominantly lipidic—accounting for approximately 70% of the seed mass—composed primarily of oleic and linoleic fatty acids (about 37% each). This is followed by proteins, starch and soluble sugars [17]. For the mineral nutrients, the most abundant macronutrients in the composition of Brazil nut seeds are P, K, Mg, and Ca, and the micronutrients present are Se, Fe, Zn, Mn, and Cu [17–19].

These primary and mineral reserves play a crucial role in seed germination. Following the onset of imbibition (the first stage of germination), protein synthesis and the formation of hydrolytic enzymes begin, initiating the metabolism of these reserves, particularly the mobilization of carbohydrates, lipids, and proteins [7,20]. The function of these reserves is to supply energy (carbohydrates and lipids) and support the synthesis of tissues required for early plant growth and development (proteins) [6,7].

Investigating the metabolism of primary and mineral reserves during the germination of *B. excelsa* allows for the identification of physiological variations among genotypes and potential biochemical markers useful for selecting superior materials. As such, this study evaluated two cultivated genotypes (606 and Santa Fé) for their potential application in ecological restoration and genetic improvement programs. Here, we hypothesize that (1) the mobilization of carbohydrates, lipids, proteins, and minerals differs between the genotypes 606 and Santa Fé, reflecting specific metabolic characteristics, and (2) these metabolic

patterns enable the identification of biochemical markers applicable to the selection of genotypes with superior performance.

## 2. Materials and Methods

### 2.1. Plant Material Collection and Processing

Fruits from two genotypes of *Bertholletia excelsa* (606 and Santa Fé = SF) were collected from 10 trees of each genotype at the Aruanã Agricultural Company S. A. (Itacoatiara/AM) (3°0'30.63" S, 58°50'1.50" W), Brazil, in January and February 2022. These trees were at least 50 m apart.

The fruits were opened using a machete to extract the seeds. These seeds then had their coats removed according to the method of Gonçalves et al. (2024) [10]. To perform seed antisepsis and minimize contamination by endophytic fungi, the embryos were subsequently submerged in a solution of garlic vine (*Mansoa alliacea* A.H. Gentry), a species known for its antifungal potential [21]. The solution was prepared with 17.2 g<sup>-1</sup>.L.FM of fresh leaves in distilled water and the embryos were submerged for 5 min. Afterward, the seeds were quickly dried on sterilized filter paper [10]. They were then air-dried at room temperature for 18 h, conditioned in impermeable plastic packaging, and then transported to the Laboratory of Plant Physiology and Biochemistry (LPPB-NIAR), where the experiments were performed.

### 2.2. Germination and Early Seedling Development Stages

The embryos were transferred to the greenhouse at the LPPB-NIAR, where the ambient temperature averaged 35 ± 2 °C. The substrate used for the germination tests was medium grain expanded vermiculite, which was previously autoclaved for 10 min at 121 °C and 1 atm. The processed embryos were then sown in the substrate. Irrigation was performed with distilled water every 48 h, to avoid fungal contamination due to water accumulation in the trays, or when the substrate appeared dry. Regarding light conditions, the trays were kept under natural light, with a photoperiod of 12 h of light/dark, and their positions were rotated weekly to ensure all seeds experienced the same environmental conditions.

Based on preliminary morphological observations of *B. excelsa* germination, seven developmental stages were established, taking into account the main structural differences between them [10]. These stages were divided into a quiescent phase, comprising the quiescent embryo (QE) stage, which was collected for analysis immediately after the removal of the seed coats; a germinative phase, which includes the imbibed embryo (IE) stage (after soaking in distilled water for 48 h); the root protrusion (RP) stage; a post-germinative phase, which includes the primary root elongation (RE); and the secondary root (SR); epicotyl emergence (EE); and expansion of leaves (Eex) stages [10] (Figure 1).

Due to the undifferentiated morphology of the *B. excelsa* seed, which lacks distinction among endosperm, cotyledons, and embryo tissues, the entire seminiferous organ was treated as the embryo, given that it corresponds to a hypocotyl-type embryo [10].

From each of the abovementioned stages, embryos and seedlings were collected, and their attached structures (tegmen remnants, hypocotyls, radicles, primary and secondary roots, epicotyls, and leaves) were removed prior to subsequent analyses of primary and mineral reserve mobilization.

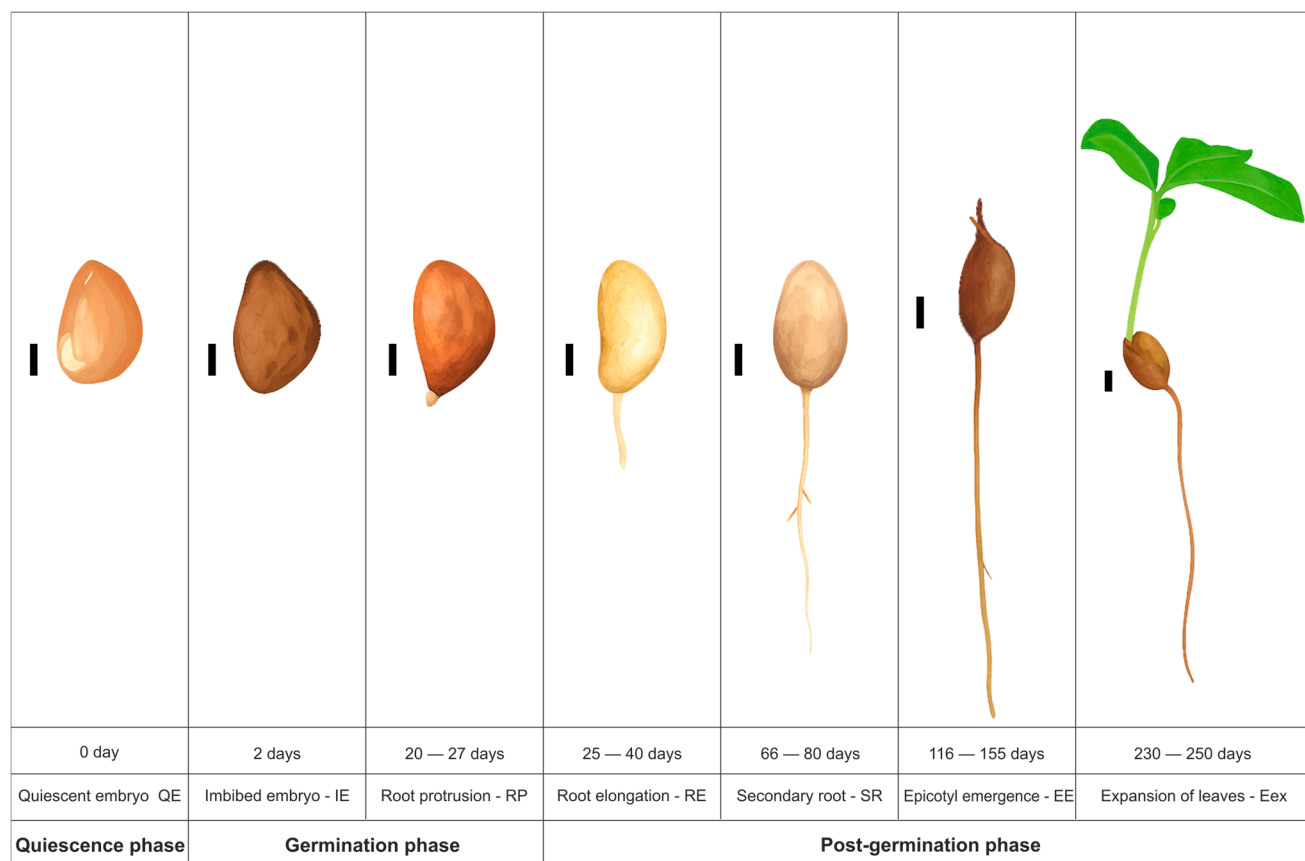


**Figure 1.** Germination and initial development stages of *Bertholletia excelsa* seeds, scalebar = 1 cm.

### 2.3. Reserve Metabolism

#### 2.3.1. Extraction and Quantification of Primary Reserves

At each germination stage, 10 embryos were collected, and their metabolic activity was immediately quenched in liquid nitrogen. The samples were then stored in a  $-80^{\circ}\text{C}$  freezer. The material was freeze-dried using a lyophilizer (CHRIST Alpha 1–4 LSC basic, São Paulo, SP, Brazil), ground in an analytical mill (Ika-Werke/M20, IKA Werke GmbH & Co. KG, São Bernardo do Campo, SP, Brazil) and stored in a  $-80^{\circ}\text{C}$  freezer until analysis.

Lipids were extracted from the samples in an ultrasonic bath (Ultronique, Q3.0/40A, Ecosonics, Indaituba, SP, Brazil) following a modified version of the method of [22]. The extraction was performed at  $30^{\circ}\text{C}$  for 30 min using n-hexane (20 mL) as the solvent. From the resulting defatted material, starch, sucrose, fructose, glucose, and soluble proteins were extracted and quantified. Starch, sucrose, fructose, and glucose were determined using an enzymatic method according to the methodology described by Fernie et al. (2001) [23].

For the extraction of soluble proteins, TRIS-HCl buffer (mM, pH 7.5) was used, while quantification was performed using the method described by Bradford (1976) [24], with absorbance read at 595 nm in a spectrophotometer. Finally, the amino acids were extracted from the samples using 1 M sodium citrate buffer, pH 5.2, supplemented with 0.2% ascorbic acid, and subsequently measured in a spectrophotometer at an absorbance of 570 nm [25].

#### 2.3.2. Extraction and Quantification of Mineral Reserves

The extraction and determination of the macronutrients phosphorus (P), potassium (K), sulfur (S), calcium (Ca), and magnesium (Mg) and the micronutrients selenium (Se), zinc (Zn), iron (Fe), manganese (Mn), copper (Cu), and boron (B) were performed using 0.5 g aliquots from each germination stage. These samples were subsequently digested with nitric acid ( $\text{HNO}_3$ ).

Next, the samples were filtered through a 0.45 µm porosity PTFE filter (Millipore®, São Paulo, SP, Brazil). After filtration, the samples were adjusted to a final volume of 50 mL via the addition of ultrapure water [26]. After these steps, the minerals were quantified using inductively coupled plasma optical emission spectrometry (ICP-OES; Shimadzu, 9820, São Paulo, SP, Brazil) [27].

## 2.4. Calculation of Metabolic Indices and Ratios for Primary and Mineral Reserves

### 2.4.1. Metabolic Flux Index (MFI)

To assess the metabolic dynamics of transient use and synthesis across the seven stages of germination and early growth, the MFI index was adapted from the principles of relative growth rate (RGR) [28,29]. The values were calculated between consecutive germination stages (QE-IE, IE-RP, RP-RE, RE-SR, SR-EE, and EE-Eex) and the proportional change (as a fold-change) in the accumulation/release or degradation/consumption of reserves between these stages was calculated using the equation:

$$MFI_i = \frac{Value_{si} - \overline{Value_{si-1}}}{\overline{Value_{si-1}}}$$

where

$MFI_i$  = Metabolic flux index between two stages

$Value_{si}$  is the value at stage i

$\overline{Value_{si-1}}$  is the mean of the replicates at stage i−1

### 2.4.2. Net Accumulation Change (NAC)

The NAC calculates the metabolic balance between the first (QE) and the last (Eex) stage. If the result is a positive value, it suggests a net accumulation of that metabolite/mineral by the end of the initial development of that genotype, i.e., there was metabolic/mineral net synthesis/release. If the result is a negative value, it signifies intense net consumption of that metabolite/mineral, i.e., it was degraded/consumed more than it was produced throughout germination. The NAC was calculated as follows:

$$NAC = E_f - \overline{E_i}$$

where

NAC = Net Accumulation Change

$E_f$  is the metabolite value at the final stage (Eex);

$\overline{E_i}$  is the mean of metabolite value at the initial stage (QE).

Total activity index (TAI)

This index is the summation of the absolute MFI values, and it assesses the strategy and total metabolic activity of a given metabolite/mineral. It integrates the absolute transient fluctuations (i.e., the differences between stages, expressed as positive values even when the change is negative) into a single final value. The results express the cumulative metabolic activity, demonstrating the total metabolic cost from the beginning to the end of early development. This index is calculated using the following equation:

$$TAI = \sum_{i=2}^n \left| \frac{Value_{si} - \overline{Value_{si-1}}}{\overline{Value_{si-1}}} \right|$$

where

TAI = Total Activity Index

$Value_{si}$  is the value at stage i

$\overline{Value_{si-1}}$  is the mean of the replicates at stage i−1

$n$  = number of germination stages evaluated

## 2.5. Experimental Design and Statistical Analyses

The experiment was conducted in a completely randomized design, arranged in a  $2 \times 7$  factorial scheme. The factors were two genotypes (606 and Santa Fé = SF) and seven germination stages (quiescent embryo = QE; imbibed embryo = IE; radicle protrusion = RP; primary root elongation = RE; secondary root = SR; epicotyl emergence = EE; and expansion of leaves = Eex). Each sample consisted of 10 randomly collected seeds at each germination stage. The quantification of primary and mineral reserves was performed using triplicate assays of samples composed of 10 embryos each, for every germination stage and genotype evaluated.

The calculated MFI values for “Starch”, “Fructose”, “Glucose”, “Se”, and “Fe” were transformed using the Yeo-Johnson transformation [30]. Subsequently, the data were subjected to the Shapiro–Wilk and Levene’s tests to verify the assumptions of normality and homogeneity of variances, respectively. A two-way analysis of variance (ANOVA) was then performed to test the effects of the two factors (genotype and germination stage) on the MFI responses. For variables that did not meet these assumptions (“Soluble proteins”, “P”, “K” and “B”), the non-parametric Kruskal–Wallis test was used.

Following significant results from the hypothesis tests ( $p < 0.05$ ), Tukey’s HSD (honestly significant difference) test was applied to compare significant differences among the mean germination stages for each metabolite within each genotype. To compare the same germination stages between the two genotypes for each MFI metabolite, as well as the NAC and TAI indices, Welch’s  $t$ -test for independent samples was used. For the comparisons that violated the aforementioned assumptions, which included the MFI of specific metabolites and the NAC for K, S, Ca, and Mg, and the TAI for K, the non-parametric equivalent, the Wilcoxon–Mann–Whitney test, was applied.

To express the intensity and direction (accumulation or degradation) of metabolism, the MFI results were normalized to a Z-score and subsequently classified as: “Intense transient synthesis/compartimentation”, when the result was a positive value  $> 1.5$ ; “Moderate transient synthesis/compartimentation”, when the result was a positive value between 0.5 and 1.5; “Intense degradation/mobilization”, when the value was a negative value  $< -1.5$ ; “Moderate degradation/mobilization”, when the value was a negative value between  $-0.5$  and  $-1.5$ ; and “Stable metabolism”, when the value was between  $-0.5$  and 0.5.

Furthermore, a principal component analysis (PCA) was performed on the raw metabolic data to examine the clustering of metabolites/minerals with the evaluated stages for both genotypes. All data processing, statistical analyses and graph creation were performed using the R programming environment [31] and the RStudio interface version 2024.12.1+563, with the exception of the PCA, which was created in PAST software version 5.3 [32].

In this study, the car package was used for testing assumptions of normality (Shapiro–Wilk) and homogeneity of variance (Levene’s test), as well as for performing Yeo–Johnson power transformations when needed. When parametric assumptions were satisfied, agricolae supported one- and two-way ANOVA and Tukey’s post hoc tests. For non-parametric testing, the Kruskal–Wallis and Dunn–Bonferroni post hoc comparisons were conducted using the FSA and rcompanion packages, respectively. Pairwise comparisons between genotypes in each stage were performed via  $t$ -tests (parametric) or Wilcoxon tests (non-parametric), as appropriate. Data wrangling and transformation relied on dplyr, tidyr and related tidyverse packages, while graphical representations were created using ggplot2 and patchwork.



### 3. Results

#### 3.1. Mobilization and Metabolism of Carbohydrate Reserves

The contents of carbohydrate reserves (starch, sucrose, fructose, and glucose) in *Bertholletia excelsa* embryos varied across the stages of germination and early development for both the genotypes 606 and Santa Fé. Furthermore, these contents also differed when comparing the genotypes at corresponding stages (Figure 2a–d). Similarly, the results for the relative metabolism of these reserves (i.e., their MFI values) revealed significant differences both between the genotypes and across the germinative and post-germinative stages (Figure 2a–d).

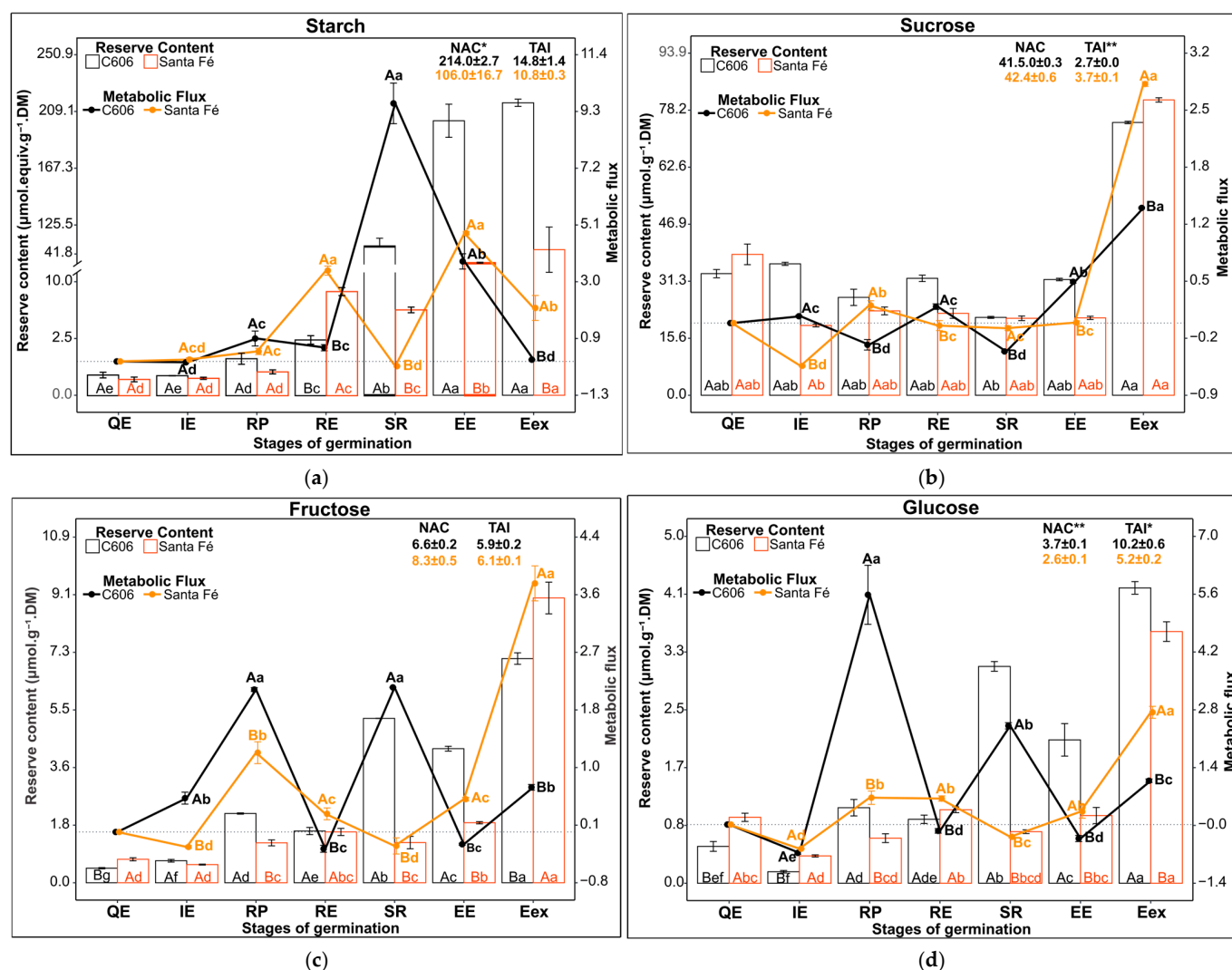


**Figure 2.** Reserve content and metabolic flux of carbohydrates of two genotypes of *Bertholletia excelsa*, (a) = starch, (b) = sucrose, (c) = fructose, and (d) = glucose. The dotted line indicates the value 0 of metabolic flux. QE = quiescent embryo stage, IE = imbibed embryo stage, RP = root protrusion stage, RE = root elongation stage, SR = secondary root stage, EE = epicotyl emergence stage and Eex = expansion of leaves stage. Capital letters are used to compare genotypes at the same stage of germination, lowercase letters are used to compare germination stages within the same genotype for a given metabolite. Same letters mean non-significant comparisons ( $p > 0.05$ ); different letters mean significant comparisons ( $p \leq 0.05$ ); NAC = net accumulation change, in  $\mu\text{mol.equiv.g}^{-1}.\text{DM}$  for the starch and in  $\mu\text{mol.g}^{-1}.\text{DM}$  for the sucrose, fructose and glucose; TAI = total activity index; \* indicates  $p$ -value  $\leq 0.05$ ; \*\* indicates  $p$ -value  $\leq 0.01$ ;  $n = 10$ .

### 3.1.1. Starch

The starch content of genotype 606 increased steadily throughout the germinative and post-germinative phases ( $p < 0.001$ ) (Figure 2a). In the Santa Fé genotype, starch levels remained unchanged during the quiescent and germinative phases, but rose significantly in the post-germinative phase ( $p < 0.001$ ). At the primary root elongation (RE) stage, Santa Fé accumulated significantly more starch than 606, around 86.7% ( $p < 0.001$ ); whereas, in the subsequent stages like secondary root (SR), epicotyl emergence (EE) and expansion of leaves (Eex) starch content was higher in 606 ( $p < 0.05$ ), 587.78, 462.7, and 100.9%, respectively (Figure 2a).

Regarding starch metabolism (Figure 2a), genotype 606 exhibited initial degradation at the onset of germination followed by transient synthesis during the post-germinative phase, with the most pronounced increases at the RP, SR, and EE stages ( $p < 0.001$ ), particularly during secondary root formation ( $p < 0.001$ ). In Santa Fé, starch degradation occurred only at the SR stage ( $p < 0.001$ ), while transient synthesis took place during the germinative and early and late post-germinative phases, with significant accumulation in the RE, EE, and Eex stages ( $p < 0.001$ ). The highest starch levels in Santa Fé were observed at the RE and EE stages.

Comparatively, transient starch synthesis was 5422.22% greater in 606 at the SR stage ( $p < 0.05$ ); whereas Santa Fé showed, respectively, 560.78 and 2728.57% higher synthesis during the RE and Eex stages ( $p < 0.05$ ) (Figure 2a). Overall, genotype 606 exhibited a significantly (101.73%) higher positive starch balance (NAC) ( $p < 0.05$ ), though total metabolic activity (TAI) did not differ between genotypes (Figure 2a).

### 3.1.2. Soluble Sugars

Sucrose, fructose, and glucose exhibited distinct accumulation trends in genotype 606 during germination. Sucrose showed a divergent pattern from the hexoses between germinative and early post-germinative stages, converging only at the end of the post-germinative phase, with significant minima and maxima in the SR and Eex stages, respectively ( $p < 0.001$ ) (Figure 2b). Fructose increased steadily throughout germination, fluctuating post-germination (Figure 2c), while glucose displayed a sharp early decline followed by similar fluctuations (Figure 2d). The lowest fructose and glucose levels in 606 occurred in the QE and IE stages, with peaks in the final post-germinative stage ( $p < 0.001$ ).

After germination, glucose concentrations rose first, followed by fructose, culminating in higher relative levels of all soluble sugars at the final stage. These increases likely reflect the conversion of reserve carbohydrates and the relative concentration effect caused by the progressive mobilization of other storage compounds, rather than the *de novo* synthesis of sugars. Santa Fé's lowest sugar concentrations occurred during quiescence and germination, with highest values at the end, paralleling 606.

Comparatively, genotype 606 accumulated higher sugars at the end of germination and in the SR and EE stages for fructose (roughly 73.5, 309.21 and 123.34%, respectively) and glucose (about 67.5, 320.5 and 111.81%, respectively); whereas Santa Fé had elevated fructose and glucose during quiescence (60.65 and 79.04%, respectively) and greater fructose accumulation terminally, close to 27.02% higher than 606 ( $p < 0.001$ ).

Metabolically, 606 synthesized sucrose and fructose early in germination, followed by fructose and glucose production at the end of germination and in the SR stage, with all sugars synthesized in the final stage, plus additional sucrose synthesis during RE and EE ( $p < 0.001$ ). Degradation events varied: glucose degraded early, sucrose at the end of germination, and both sugars sporadically during post-germinative stages, often alternately, with glucose degradation peaking during IE ( $p < 0.001$ ).



Santa Fé showed degradation of all soluble sugars early and during SR, with transient synthesis at germinative and post-germinative endpoints. Post-germination began with sucrose degradation and fructose/glucose synthesis, followed by degradation during SR and elevated synthesis during the EE and Eex stages ( $p < 0.001$ ). Transient synthesis peaked during Eex, while early germination featured maximal sucrose and glucose degradation (Figure 2b–d).

Between the genotypes, fructose synthesis during RP was 79.8% greater in 606 ( $p < 0.001$ ), while Santa Fé synthesized 558.20% more soluble sugars in the final stage ( $p < 0.001$ ). Antagonistic metabolic patterns were evident for all sugars in the RE and EE stages, with differences in sucrose and fructose at IE and sucrose during RP.

Net accumulation change (NAC) of sucrose and fructose did not differ significantly between genotypes; however, glucose NAC was significantly higher in 606 (about 39.21%), indicating a superior positive metabolic balance ( $p < 0.001$ ) (Figure 2d). The total activity index (TAI) revealed contrasting patterns: sucrose metabolism was 63.60% higher in Santa Fé ( $p < 0.01$ ), whereas glucose metabolism predominated in 606 (about 39.20%) (Figure 2b,d).

### 3.2. Mobilization and Metabolism of Lipid Reserves

Lipid content in the embryos of the genotypes 606 and Santa Fé varied during post-germinative stages, though quantities were comparable in the corresponding stages (Figure 3). Within-genotype analysis revealed stage-specific metabolic differences. In genotype 606, lipid levels remained stable across the first five stages, declining from epicotyl emergence (EE) onwards. Similarly, Santa Fé maintained stable lipid reserves through six stages, with slight increases during IE and RP, followed by a significant decrease in the final stage (Figure 3).

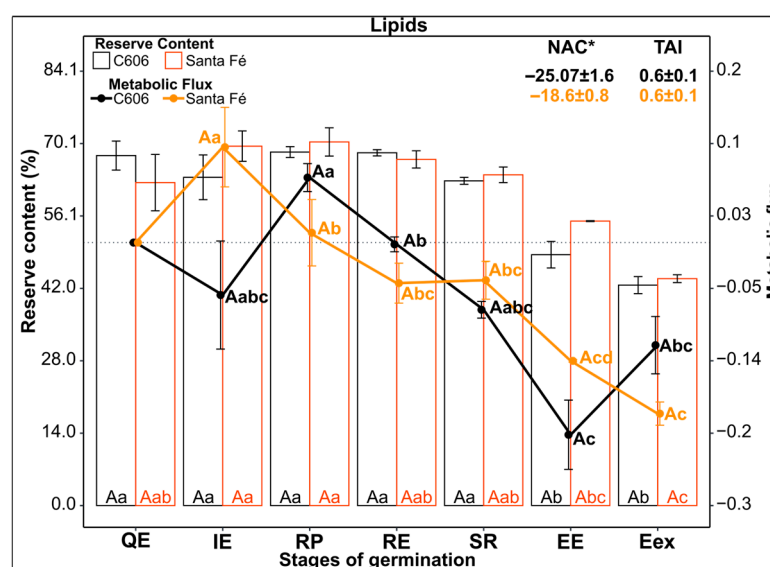


**Figure 3.** Reserve content and metabolic flux of lipids of two genotypes of *Bertholletia excelsa*. The dotted line indicates the value 0 of metabolic flux. QE = quiescent embryo stage, IE = imbibed embryo stage, RP = root protrusion stage, RE = root elongation stage, SR = secondary root stage, EE = epicotyl emergence stage and Eex = expansion of leaves stage. Capital letters are used to compare genotypes at the same stage of germination, lowercase letters are used to compare germination stages within the same genotype for a given metabolite. Same letters indicate non-significant comparisons ( $p > 0.05$ ); different letters indicate significant comparisons ( $p \leq 0.05$ ); NAC = net accumulation change, in percentage; TAI = Total Activity Index; \* indicates  $p$ -value  $\leq 0.05$ ;  $n = 10$ .

Lipid metabolism proceeded similarly in both genotypes, yet distinct features emerged during germination and early seedling growth. Genotype 606 showed lipid accumulation

only during RP, stable metabolism during RE, and progressive degradation in the IE, SR, EE, and Eex stages, peaking during EE (Figure 3). Santa Fé accumulated lipids during IE and RP but experienced continuous degradation thereafter, reaching its maximum in the expansion of leaves stage ( $p < 0.001$ ) (Figure 3).

Despite overall lipid content similarity, transient lipid synthesis occurred during IE in Santa Fé contrasting with degradation in 606; metabolism during RE was null in 606 but showed degradation in Santa Fé (Figure 3). Final metabolic balance (NAC) indicated lipid degradation in both genotypes, significantly greater in 606 (about 41.56%) ( $p < 0.05$ ), while total activity index (TAI) was comparable between them (Figure 3).

### 3.3. Mobilization and Metabolism of Proteins and Amino Acids Reserves

Soluble protein concentrations fluctuated throughout early development in genotypes 606 and Santa Fé, with pronounced differences at specific stages, especially during quiescence, initial emergence, and radicle protrusion, where Santa Fé consistently showed higher values ( $p < 0.01$ ) (Figure 4a). Amino acid contents varied among developmental stages within each genotype, but remained statistically similar across genotypes at corresponding stages (Figure 4b).

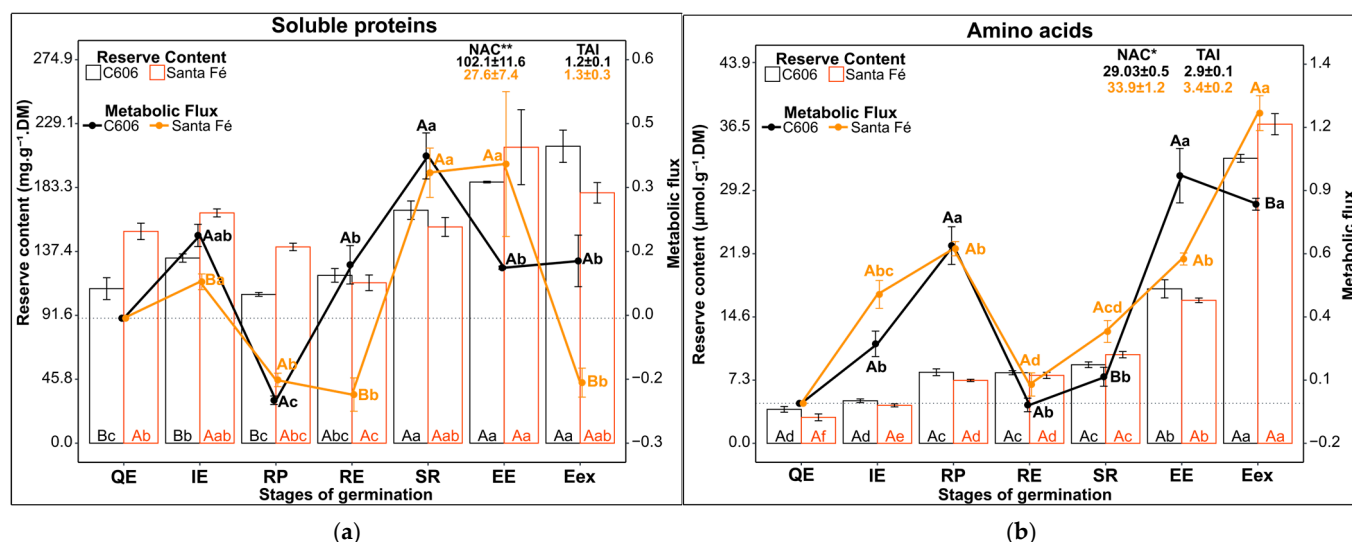


**Figure 4.** Reserve content and metabolic flux of proteins of two genotypes of *Bertholletia excelsa*, (a) = soluble proteins, (b) = amino acids. The dotted line indicates the value 0 of metabolic flux. QE = quiescent embryo stage, IE = imbibed embryo stage, RP = root protrusion stage, RE = root elongation stage, SR = secondary root stage, EE = epicotyl emergence stage, and Eex = expansion of leaves stage. Capital letters are used to compare genotypes at the same stage of germination, lowercase letters are used to compare germination stages within the same genotype for a given metabolite. Same letters indicate non-significant comparisons ( $p > 0.05$ ); different letters indicate significant comparisons ( $p \leq 0.05$ ); NAC = net accumulation change, in mg.g<sup>-1</sup>.DM for the soluble proteins, and in μmol.g<sup>-1</sup>.DM for the amino acids; TAI = total activity index; \* indicates  $p$ -value  $\leq 0.05$ ; \*\* indicates  $p$ -value  $\leq 0.01$ ;  $n = 10$ .

#### 3.3.1. Soluble Proteins

In genotype 606, protein levels changed dynamically during the first three phases, increasing significantly with secondary root stage and remaining elevated through the final stages, though differences among the last three phases were not significant (Figure 4a). Santa Fé mirrored this early dynamic, with a quantity of soluble proteins 37.1, 24.36 and 31.9% higher in the first three stages, respectively, than genotype 606; but it experienced a marked decrease from RP to RE. From primary root elongation onwards, the increase in protein resembled what was observed in 606.

Regarding metabolic mobilization, soluble protein synthesis in 606 was evident during IE, RE, SR, EE, and Eex, peaking at SR ( $p < 0.001$ ), with moderate increases during RE, EE and Eex, and with degradation restricted to the RP stage (Figure 4a). In Santa Fé, synthesis was present during IE, SR, and EE, most intensely at SR and EE, and weakest at IE; while the RP, RE, and Eex stages saw similar levels of protein degradation (Figure 4a).

When comparing genotypes, both exhibited protein synthesis during IE, SR, and EE; despite this, 606 surpassed Santa Fé in the IE stage ( $p < 0.05$ ), with similar profiles during SR and EE (Figure 4a). In the RP stage, both underwent degradation; however, during RE and Eex, 606 synthesized proteins while Santa Fé degraded them. In the final assessment, both genotypes had a positive net accumulation (NAC) of soluble proteins, with 606 amassing significantly greater reserves, whereas total metabolic activity (TAI) was comparable in both (Figure 4a).

### 3.3.2. Amino Acids

In genotype 606, amino acid levels increased significantly during the RP, EE, and Eex stages ( $p < 0.001$ ) (Figure 4b). In Santa Fé, significant increases occurred in nearly all stages except RE ( $p < 0.001$ ). Amino acid synthesis in 606 was most pronounced during RP, EE, and Eex ( $p < 0.001$ ), followed by similar but lower activity during IE, RE, and SR (Figure 4b). In Santa Fé, synthesis peaked significantly in Eex ( $p < 0.001$ ), with comparable intensities during IE, RP, and EE, and lower activity in RE and SR. Notably, Santa Fé accumulated more amino acids than 606 in the SR and Eex stages (nearly 181.82 and 44.71%, respectively).

The net accumulation change (NAC) indicated amino acid accumulation in both genotypes, with Santa Fé exhibiting significantly greater accumulation ( $p < 0.05$ ) (Figure 4b). Total metabolic activity (TAI) was statistically similar between the two (Figure 4b).

## 3.4. Mobilization and Metabolism of Mineral Reserves

### 3.4.1. Macronutrients and Selenium

The levels of phosphorus (P), potassium (K), sulfur (S), calcium (Ca), magnesium (Mg), and selenium (Se) varied in the germinative and post-germinative stages in genotypes 606 and Santa Fé, with significant differences both within and between genotypes (Figure 5a–f).

In genotype 606, Se alone increased significantly at the onset of germination ( $p < 0.001$ ), followed by declines at the end of the stage for Se, S and Ca ( $p < 0.05$ ). Post-germination, Ca declined in the SR and EE stages, alongside S and Se in EE, while P, S, Mg and Se increased in the final stage ( $p < 0.05$ ).

During quiescence, 606 showed elevated S and Ca levels ( $p < 0.05$ ), with Ca remaining high into early germination and lowest in the EE and late stages, paralleling Se's minimum in the final stage. Mg and P peaked late post-germination, while P was lowest during RE, and Mg during SR. Santa Fé only exhibited significant mineral changes post-germination, with increased P and Mg late and Se in SR, alongside decreases in Se during RE and late stages, and a reduction in Ca during EE.

Santa Fé consistently registered higher Se during quiescence (around 86.34%), elevated S in early and late germination (approximately 12.20%, considering the mean of the IE, RP and RE stages for both genotypes), 7.44 and 8.53%, respectively, greater Mg during RE and in the penultimate stages. Conversely, 606 exceeded Santa Fé in 8.3% for the Ca only during late development.

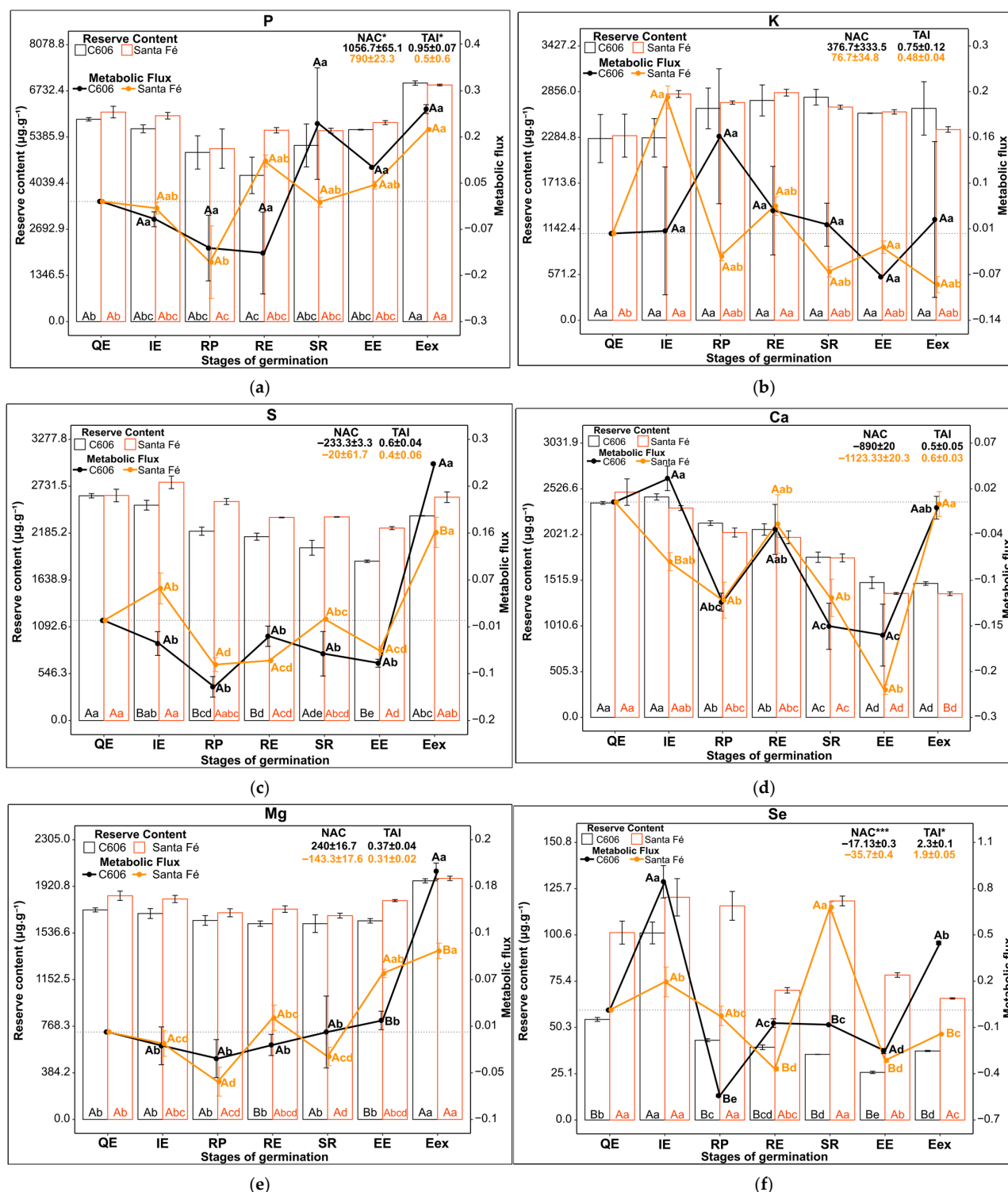


**Figure 5.** Reserve content and metabolic flux of macronutrients and selenium in two genotypes of *Bertholletia excelsa*, (a) = phosphorus (P), (b) = potassium (K), (c) = sulfur (S), (d) = calcium (Ca), (e) = magnesium (Mg) and (f) = selenium (Se). The dotted line indicates the value 0 of metabolic flux. QE = quiescent embryo stage, IE = imbibed embryo stage, RP = root protrusion stage, RE = root elongation stage, SR = secondary root stage, EE = epicotyl emergence stage and Eex = expansion of leaves stage. Capital letters are used to compare genotypes in the same stage of germination; lowercase letters are used to compare germination stages within the same genotype for a given metabolite. Same letters indicate non-significant comparisons ( $p > 0.05$ ); different letters indicate significant comparisons ( $p \leq 0.05$ ); NAC = net accumulation change, in  $\mu\text{g.g}^{-1}$ ; TAI = Total Activity Index; \* indicates  $p\text{-value} \leq 0.05$ ; \*\*\* indicates  $p\text{-value} \leq 0.001$ ;  $n = 10$ .

Macro mineral metabolism in 606 showed net consumption of P, S and Mg throughout germination, while Ca and Se displayed net release initially, with subsequent significant mobilization. Post-germination featured mineral consumption except for K, with significant Se consumption; P was released uniformly late, Ca consumption peaked in SR, K fluctuated, S was consumed throughout EE, then released significantly, Mg was released late, and Se exhibited alternating consumption and release.

Santa Fé's early germination involved net P, Ca, and Mg consumption and K, S, and Se release; late germination maintained this pattern with significance for S and Mg only. Post-germination began with the release of P, K, and Mg (significant for Mg), and consumption of S, Ca, and Se (significant for Se). Late stages saw P release, K and Ca consumption (significant during EE, SR, and Eex), dynamic S metabolism, Mg consumption then release, and inverse trends for Se.

Genotypic differences included 81.25% higher S release by 606 in Eex, 352.63% greater Se release by 606 in early germination and 1325% consumption in RP; respectively, 333.33 and 25.93% higher Santa Fé consumption in RE and EE for Se, and antagonistic Se metabolism in SR and Eex. Santa Fé released 600% more Mg during EE, while 606 released 100% more Mg late. Significant NAC differences showed genotype 606, 33.75% superior in P accumulation ( $p < 0.05$ ) and Santa Fé 108.59% greater Se consumption ( $p < 0.001$ ). TAI mirrored NAC trends, with 606 showing, respectively, 44 and 25% higher metabolic activity for P and Se. K was the only mineral with consistent positive accumulation; others, including Se, had negative final balances.

### 3.4.2. Micronutrients

The concentrations of zinc (Zn), iron (Fe), manganese (Mn), copper (Cu) and boron (B) exhibited variable patterns during germination and early development in 606 and Santa Fé, with notable intra- and inter-genotype differences (Figure 6a–e).

In 606, Zn and Cu increased significantly early in germination ( $p < 0.05$ ), while all micronutrients decreased at the end of the stage, particularly Zn, Mn, and Cu ( $p < 0.05$ ). Post-germinative mineral levels were largely stable except for significant late Mn fluctuations ( $p < 0.05$ ).

During quiescence, Fe and Mn peaked significantly ( $p < 0.05$ ), with Zn and Cu at their highest at the onset of germination. Minimal concentrations appeared during distinct post-germinative stages for each mineral: Zn in RE and EE; Fe and Cu in EE; Mn in Eex. Santa Fé showed stable Zn, Fe, and Cu throughout; Mn declined significantly during IE, SR and EE ( $p < 0.05$ ); and B increased significantly only early on in germination. Mn was highest in quiescence and early post-germination, lowest in late germination; Fe peaked late and was lowest in RE; B was absent during quiescence and peaked in late germination.

For Zn and Cu, Santa Fé generally exhibited 70.8 and 76.6%, respectively, higher Zn and Cu abundances in all stages (considering a comparative analysis of the averages in all stages for both genotypes), while 606 showed 57.6% elevated Fe post-germination (considering an average in the RP to Eex stages for both genotypes), and 121.4% higher Mn across the stages, and along with 380% higher B in quiescence stage.

Metabolically, 606's post-germinative phase displayed only net Mn consumption; Zn, Fe, Cu, and B shifted from net release early to net consumption late, with Zn and Cu consumption being significant ( $p < 0.05$ ). Cu showed a significant net release early post-germination. Late stages involved significant Zn and Fe release ( $p < 0.05$ ), concurrent significant Mn and Fe consumption, significant Mn release in EE, and significant consumption of other minerals except B. The final stage reversed these trends significantly, sparing B.



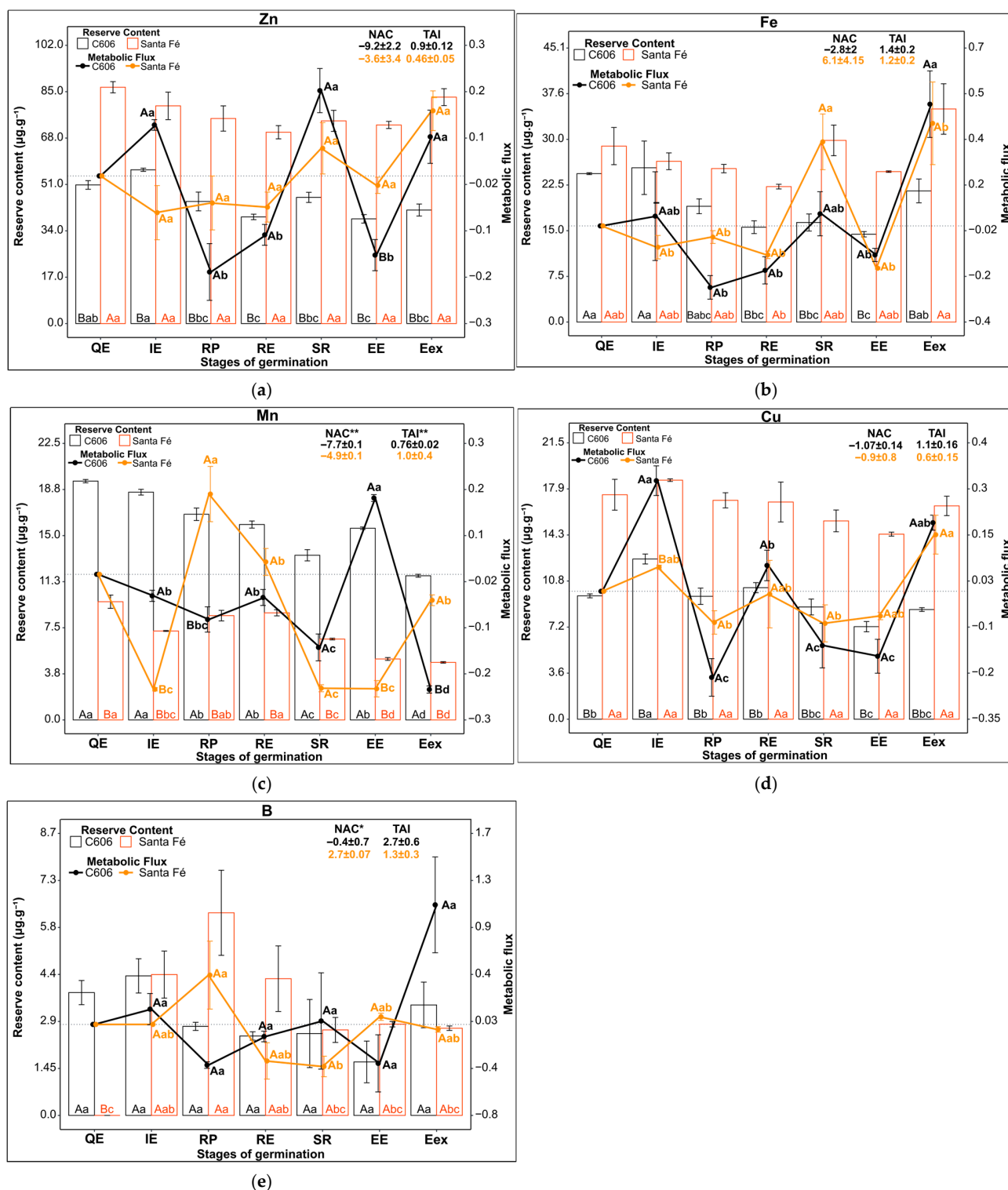


**Figure 6.** Reserve content and metabolic flux of micronutrients of two genotypes of *Bertholletia excelsa*, (a) = zinc, (b) = iron, (c) = manganese, (d) = copper, and (e) = boron. The dotted line indicates the value 0 of metabolic flux. QE = quiescent embryo stage, IE = imbibed embryo stage, RP = root protrusion stage, RE = root elongation stage, SR = secondary root stage, EE = epicotyl emergence stage and Eex = expansion of leaves stage. Capital letters are used to compare genotypes at the same stage of germination; lowercase letters are used to compare germination stages within the same genotype for a given metabolite. Same letters indicate non-significant comparisons ( $p > 0.05$ ); different letters indicate significant comparisons ( $p \leq 0.05$ ); NAC = net accumulation change, in  $\mu\text{g.g}^{-1}$ ; TAI = total activity index; \* indicates  $p$ -value  $\leq 0.05$ ; \*\* indicates  $p$ -value  $\leq 0.01$   $n = 10$ .

Santa Fé's Zn and B metabolism remained largely unchanged; net Zn consumption occurred during germination and in EE, with intermittent release. B showed release in RP and EE, and consumption in RE, SR, and Eex. Early germination entailed net Mn, Fe consumption, and Cu release; significant Mn release occurred late germination, while Fe fluctuated, and Cu showed significant consumption and release in varying stages.

Genotypes differed significantly in Cu and Mn release during IE and EE ( $p < 0.05$ ), with Santa Fé consuming 435.2% more Mn in IE and genotype 606 about 343.52% more in Eex. Santa Fé accumulated Mn in RP, while 606 consumed Mn, as well as 750% more Zn in EE. Significant NAC differences favored genotype 606 around 56% more negative Mn balance and Santa Fé's positive B balance. Fe NAC showed genotypic trends consistent with accumulation in Santa Fé and depletion in 606. Santa Fé exhibited significantly greater Mn metabolic activity (TAI) (31.4%) after all stages ( $p < 0.01$ ).

### 3.5. Total Mobilization and Metabolism

Distinct differences in metabolic intensities were observed between 606 and Santa Fé in germination and early development stages, with clear genotype- and stage-specific grouping patterns. In genotype 606, transient synthesis of starch and glucose peaked markedly during the secondary root stage and radicle protrusion stages, respectively. In contrast, Santa Fé exhibited pronounced soluble sugar (sucrose and fructose) metabolism during the final stage (Figure 7). Lipid metabolism was characterized by intense degradation in RP in 606, whereas Santa Fé showed strong lipid synthesis in IE. Soluble protein metabolism in 606 was moderate in RP and SR, while Santa Fé's activity remained moderate throughout the last four stages. Amino acid metabolism occurred moderately during RE, EE, and Eex in 606 and in Eex in Santa Fé (Figure 7).

Regarding minerals, a greater intensity of compartmentalization was observed in genotype 606, primarily in the final stage, with the exception of Ca, which was only moderate. In the Santa Fé genotype, however, the intensity was more pronounced for K, Ca, Se, Fe, and Mn (Figure 7).

Approximately 39.7% of the total variance is explained by the first principal component (PC1), which is likely driven primarily by the minerals Fe, Zn and Mn (Figure 8). Meanwhile, 28.6% of the variance can be explained by the second principal component (PC2), which appears to be associated with amino acids, starch, fructose, glucose, sucrose, soluble proteins, lipids, and Ca (Figure 8).

Mineral content generally exhibited higher intensity in genotype 606, particularly in the final stage, with the exception of calcium (Ca), which showed moderate levels. In Santa Fé, elevated intensities were observed primarily in potassium (K), Ca, selenium (Se), iron (Fe) and manganese (Mn) (Figure 8).

The principal component analysis (PCA) explained approximately 39.7% of the variance with the first component (PC1), predominantly driven by Fe, zinc (Zn) and Mn. The second component (PC2) accounted for 28.6% of the variance, mainly associated with amino acids, starch, fructose, glucose, sucrose, soluble proteins, lipids, and Ca (Figure 8). The variables most positively correlated in the upper-left quadrant (negative PC1, positive PC2) include Zn, sulfur (S), copper (Cu), Se, boron (B), and Ca, with B exerting a lesser influence. Lipids and Mn clustered together in the lower-left quadrant, while Mg, P, sucrose, soluble proteins, and amino acids grouped in the upper-right quadrant. Fructose, glucose, and starch clustered in the lower-right quadrant (Figure 8).

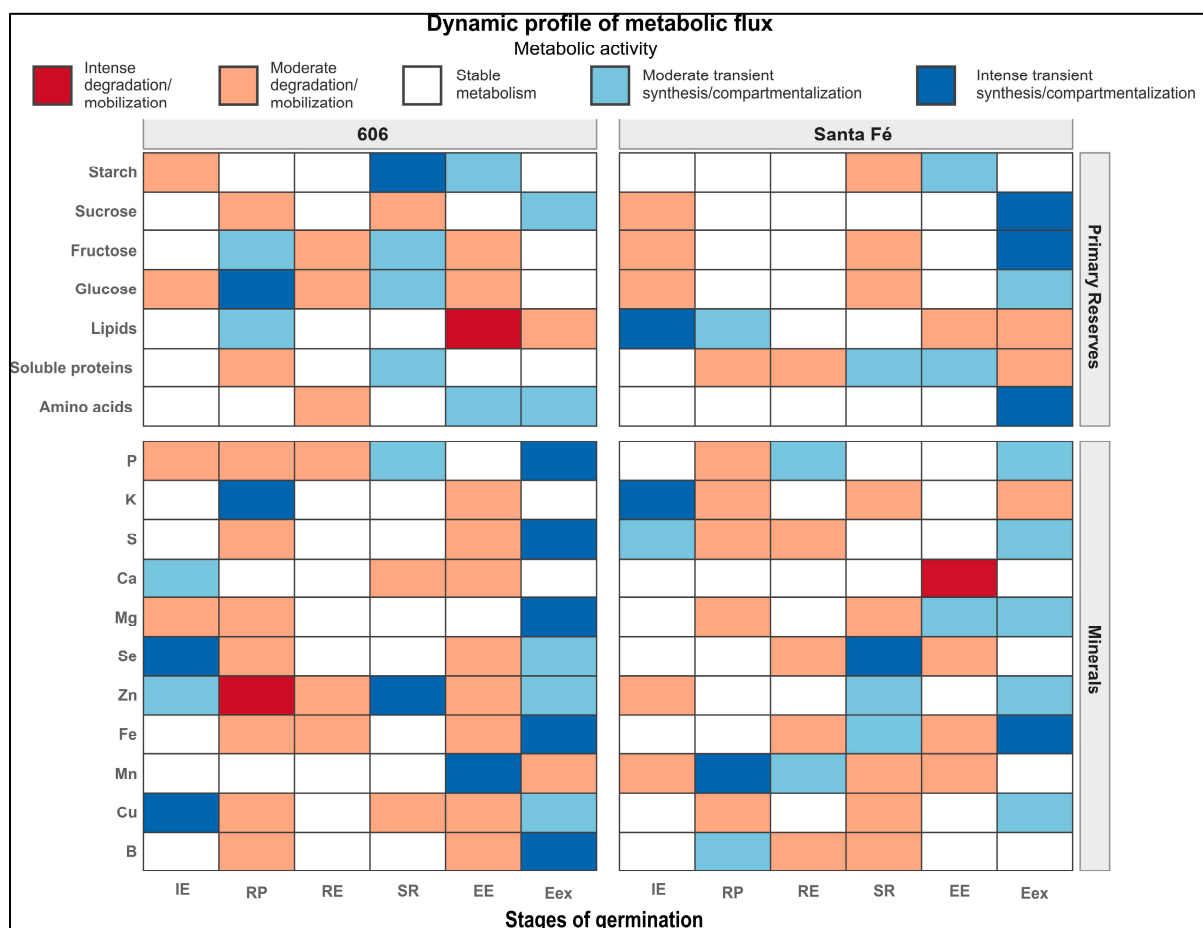


**Figure 7.** Heatmap indicating metabolic flux and intensities throughout germination and early development of two *Bertholletia excelsa* genotypes; IE = imbibed embryo stage, RP = root protrusion stage, RE = root elongation stage, SR = secondary root stage, EE = epicotyl emergence stage and Eex = expansion of leaves stage;  $n = 10$ .

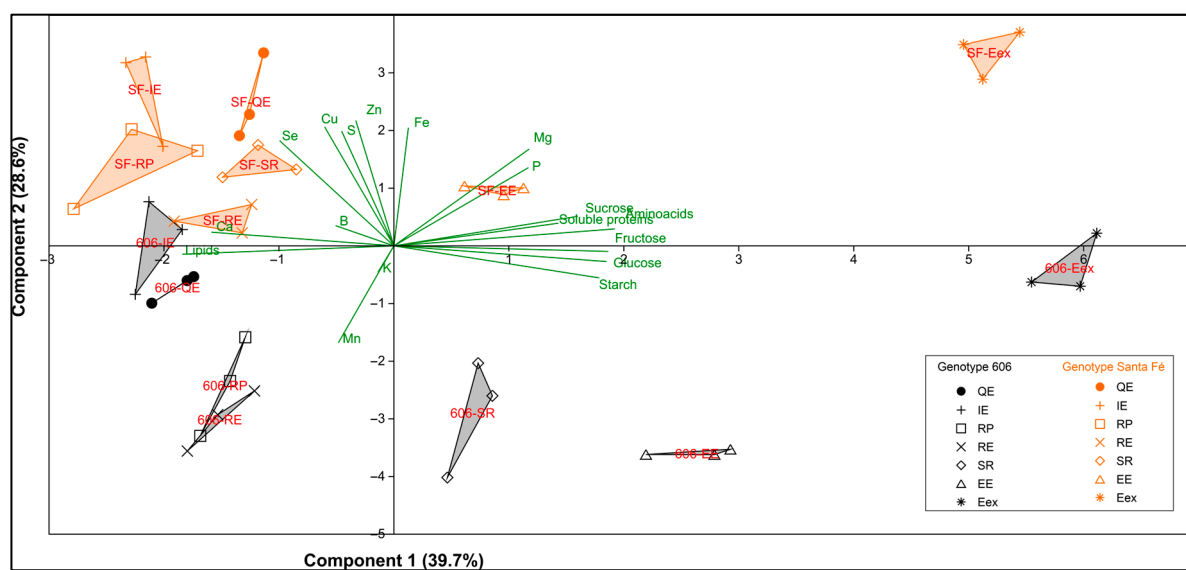


**Figure 8.** Principal component analysis (PCA) of primary metabolites and minerals in seeds of two *Bertholletia excelsa* genotypes throughout seven germination stages, QE = quiescent embryo stage, IE = imbibed embryo stage, RP = root protrusion stage, RE = root elongation, SR = secondary root stage, EE = epicotyl emergence stage and Eex = expansions of leaves stage;  $n = 10$ .

The stages of Santa Fé showed more cohesive clustering, whereas the stages of 606 were more dispersed. Notably, the QE, RP, and RE stages of 606 aligned with lipids, Mn and K; the IE stage was positioned between the two left quadrants of PC1. The SR and EE stages of 606 aligned closer to starch, glucose and fructose, with Eex situated between the upper and lower right quadrants. The first five stages of Santa Fé correlated strongly with Zn, S, Cu, Se, Ca, and B, with the latter exerting minimal influence. The last two stages closely associated with Fe, Mg, P, sucrose, soluble proteins, and amino acids (Figure 8).

The PCA clustering reinforces stage differentiation, with QE, RP, and RE positioned in opposite regions. Later stages for both genotypes clustered further apart, positioned in opposite regions along the PC2 axis.

## 4. Discussion

### 4.1. Mobilization and Metabolism of Carbohydrates Reserves

The dynamics, intensities and metabolic activities observed reveal distinct strategies in starch and soluble sugar utilization during germination and early seedling growth stages of the *Bertholletia excelsa* genotypes 606 and Santa Fé. Although carbohydrates were found in smaller quantities than lipids and proteins in the quiescent embryos, their metabolism was notably active.

Carbohydrates were the first primary reserves degraded in both genotypes, occurring between the quiescent and imbibed embryo stages, highlighting their role as an initial energy source driven mainly by  $\alpha$ -amylase activation during this period [20,33,34]. However, the carbohydrate sources employed differed between genotypes during initial germination. During imbibition, genotype 606 relied on starch to supply germination energy, followed by sucrose degradation from root protrusion to secondary root stage, then fructose and glucose degradation during root elongation and epicotyl emergence. Starch synthesis resumed at the secondary root stage to support epicotyl emergence and leaf expansion.

In contrast, the Santa Fé genotype likely metabolized quiescent starch into soluble sugars during imbibition, which sustained metabolism until secondary root stage. Late early-growth stages probably involved reserve accumulation for subsequent seedling development.

Based on these patterns, genotype 606's early germinative phase functions as a starch and glucose sink, transitioning to a starch source post-germination. The metabolic products that occur in the stages of root protrusion and emission of secondary roots serve as a source of sucrose and simpler sugars, while root elongation and epicotyl emergence act as simple sugar sinks and sucrose sources. The final stage seeks all carbohydrates. Conversely, the metabolism that occurs in most stages of the Santa Fé genotype may play a role in making starch available across all stages except secondary root stage, which along with the germinative onset, are soluble sugar sinks; the products of the stages of root protrusion, epicotyl emergence and expansion of the first pair of leaves are soluble sugar sources, while the root elongation stage drains sucrose while synthesizing fructose and glucose.

These differences in carbohydrate utilization suggest inherent structural differences in starch, such as granule architecture, between the genotypes, which directly influence mobilization efficiency and germination success [34,35]. Following initial starch mobilization, degradation dynamics in sink stages underscore starch's pivotal carbon and energy role during early development, either fueling intracellular respiration and growth or being converted into sucrose [35].

Between the two genotypes, Santa Fé synthesized more starch at the start and end of the post-germinative phases, reinforcing starch's importance in providing soluble sugars for secondary root and leaf formation. Conversely, genotype 606 showed more intense sucrose and fructose synthesis during epicotyl emergence and radicle protrusion, respectively, suggesting fructose accumulation results from sucrose degradation in 606 while

sucrose synthesis predominates in Santa Fé in this stage. Furthermore, enhanced sucrose synthesis in 606 from fructose and glucose during epicotyl emergence aligns with this degradation pattern.

These findings indicate genotype-specific strategies in carbohydrate partitioning for energy and carbon supply during tissue development, with starch and sucrose playing complementary roles in carbon metabolism linked to root, epicotyl, and leaf formation [35–37]. Notably, 606 maintains a dynamic equilibrium of transient carbohydrate synthesis and degradation, while Santa Fé favors greater reserve degradation during early germinative and post-germinative stages, highlighting the influence of genotype and environmental conditions on carbon-source metabolism [34].

Regarding accumulation (NAC) and metabolic activity (TAI), genotype 606 accumulated significantly more starch and glucose; while fructose and sucrose accumulated similarly between genotypes. A comparable TAI for starch and fructose between the genotypes suggests similar metabolic investment. The higher starch accumulation efficiency in 606 implies superior starch conversion. In contrast, Santa Fé's higher metabolic activity for sucrose, despite similar accumulation, suggests lower enzymatic efficiency. For glucose, both NAC and TAI were significantly greater in 606, indicating the intense metabolic cost underlying its accumulation.

#### 4.2. Mobilization and Metabolism of Lipid Reserves

Lipids were the predominant reserves in the seeds of genotypes 606 and Santa Fé, which exhibited distinct strategies of transient synthesis and degradation during germination and early seedling growth. The average lipid content was  $67.7 \pm 2.8\%$  in genotype 606 and  $62.5 \pm 5.5\%$  in Santa Fé in quiescent seeds, aligning with data reported by Gonçalves et al. [17].

In genotype 606, lipid metabolism was minimal between the quiescence and imbibition stages, with lipogenesis initiating only during radicle protrusion. Metabolism then remained steady until eophyll emergence, followed by intense lipid degradation and moderate degradation during the expansion of the first pair of leaves.

Conversely, Santa Fé showed intense lipogenesis from quiescence to imbibition, with moderate synthesis continuing until radicle protrusion. Little lipid metabolism was observed during the primary and secondary root stages, with moderate degradation in the final stages.

These patterns indicate progressive lipid degradation culminating with eophyll expansion. Genotype 606 underwent a single phase of moderate lipogenesis but intense degradation with eophyll emergence, while Santa Fé experienced two phases of synthesis and moderate degradation.

Storage lipids, primarily triacylglycerols within lipid bodies, degrade before autotrophic growth, corroborating the high lipid metabolism seen late in germination [38]. Similar early lipogenesis has been reported in seeds of *Simmondsia chinensis*, with reserves synthesized pre-germination and degraded thereafter [39]. The authors suggest that these reserves are synthesized in the pre-germinative stages and are degraded as the germination stages proceed. In *Hevea* genotypes, lipid degradation spans from early stages to leaf emergence, a pattern differing from the accumulation-then-degradation observed here for *B. excelsa* [6]. The more common pattern of degradation for this reserve was observed in *B. excelsa* seeds in this study, as they were accumulated in the initial stages and markedly degraded in the final stages for both genotypes.

In *Carapa* species, lipid content and metabolism remain stable, highlighting the role of lipids in stress tolerance and energy supply [7]. A similar pattern was found in the genotypes 606, and Santa Fé, and Carvalho et al. (2024) [7] emphasize that high lipid levels



can be linked to the adaptation and survival of plant species, primarily as an energy source that can be utilized under adverse conditions.

Early lipogenesis may reflect lipid remodeling that is essential for membrane maintenance and protection against cytotoxic intermediates generated by germination stress [40,41]. While some Euphorbiaceae mobilize lipids immediately after imbibition, *B. excelsa* depletes carbohydrates first, initiating lipid metabolism during radicle protrusion. Our findings on initial lipid synthesis align with those for *Jatropha curcas* [6,42], underscoring species-specific lipid metabolic dynamics despite high reserve contents and botanical affinities. Final metabolic balance (NAC) indicates greater lipid degradation in genotype 606, although equivalent metabolic effort (TAI) suggests superior efficiency in utilizing energy reserves, supporting early seedling development in *B. excelsa*.

#### 4.3. Mobilization and Metabolism of Proteins and Amino Acids Reserves

Soluble proteins were the second most abundant reserves in the quiescent embryos of *B. excelsa*. These reserves were metabolized with different dynamics in both genotypes. In genotype 606, metabolic activity was observed only in the radicle protrusion and secondary root formation stages, in which moderate degradation was noted in the former and moderate accumulation in the latter. This pattern for proteins appeared to influence the subsequent metabolism of amino acids, since a moderate degradation of amino acids was observed during primary root elongation, followed by moderate accumulations in the epicotyl emergence and eophyll expansion stages.

The Santa Fé genotype showed a soluble protein metabolic pattern that diverged from 606 at the beginning and end of the post-germinative phase. In contrast, in these stages, greater amino acid synthesis was observed, suggesting that, in both, the demand for monomers to synthesize new proteins and tissues is higher in Santa Fé for primary root and leaf development. Furthermore, the higher soluble protein content in the quiescent and germinative phases of this genotype was sufficient to sustain amino acid metabolism throughout the entire post-germinative development.

Our results show a transient synthesis of soluble proteins at the beginning of the germinative phase in both genotypes (Figure 4a). This metabolism is of great importance for the synthesis of new amino acids, as these monomers are crucial for building new tissues and proteins. However, the availability of amino acids in the initial stages is low, highlighting the need for the degradation of storage proteins during this phase, especially during imbibition, to provide the necessary resources for seedling development [43–45].

The results show that soluble protein and amino acid metabolism in genotype 606 followed a linear and directly proportional pattern of transient synthesis and degradation. In stages in which there was degradation of soluble proteins, a subsequent degradation of amino acids was maintained; and in the stage in which de novo protein synthesis occurred, this synthesis was maintained for amino acids in the next stage. This suggests that, for this genotype, soluble proteins are metabolized first, setting the stage for the subsequent metabolism of amino acids. Furthermore, it was observed that, in this genotype, soluble proteins are more in demand for radicle protrusion, while amino acids are more required for primary root elongation. In contrast, the metabolism of soluble proteins in the genotype Santa Fé is directed towards radicle protrusion, primary root elongation and the expansion of the first pair of leaves.

Soluble proteins and amino acids have antagonistic yet complementary metabolic roles, especially in the initial stages of plant development. During the germination period, amino acids are biosynthesized from storage proteins present in the seeds, even if on a smaller scale, to support the biosynthesis of new proteins that will be used for plant growth. These

new proteins can, in turn, be degraded back into amino acids, which are then converted into  $\text{CO}_2$ ,  $\text{NH}_4^+$ , and  $\text{H}_2\text{S}$  in what is known as protein metabolic turnover [34,46,47].

It was observed that the stages in which soluble protein and amino acid metabolism were most relevant for genotype 606 were: secondary root stage (soluble proteins) and eophyll emergence and eophyll expansion (amino acids). For the genotype Santa Fé, the SR and EE stages had a greater contribution to soluble protein metabolism, while the final stage had greater relevance for amino acid metabolism.

At the end of the stages, genotype 606 had synthesized more soluble proteins, while Santa Fé had synthesized more amino acids. However, the total metabolic activity (TAI) was similar for both genotypes, for both soluble proteins and amino acids. This suggests that genotype 606 is more efficient at accumulating soluble proteins, while Santa Fé is more efficient at accumulating amino acids.

The protein synthesis observed in the secondary root stage may be due to de novo synthesis from amino acids that were degraded in the previous stages, with respect to genotype 606. However, this pattern was not observed in Santa Fé, in which metabolism was noted only for soluble proteins, while amino acid accumulation occurred only in the final evaluated stage [43].

#### 4.4. Mobilization and Metabolism of Macronutrients and Se Reserves

The most abundant minerals in the initial stage were phosphorus (P), potassium (K), sulfur (S), calcium (Ca), magnesium (Mg), and selenium (Se), all showing distinct metabolic dynamics throughout germination stages and between genotypes.

Phosphorus plays a pivotal role in germination metabolism due to its presence in key molecules including ATP, UTP, CTP, and GTP, which provide energy and facilitate synthesis and metabolism of nucleic acids, phospholipids, and polymers such as sucrose, starch and cellulose. Accordingly, P is stored abundantly as phytic acid in seeds [48–50].

Potassium is crucial for osmotic regulation, enzymatic cofactor activity, and turgor pressure management, significantly contributing to water uptake and cell elongation. Our findings align with this, since K accumulated in the early stages and was metabolized during eophyll emergence in genotype 606 and during radicle protrusion, secondary root and expanded seedling stages in Santa Fé, indicating greater K demand in the latter [51,52].

The macronutrients P, K, Ca, Mg, and S are essential for seedling root development, and this is consistent with the marked mobilization observed during radicle protrusion and elongation in both genotypes. Moreover, S and Mg are linked to germination success, with low levels correlating with failure; although Santa Fé had higher overall S and Mg contents, genotype 606 consumed more S during imbibition and radicle protrusion and released more of both minerals in the final stage (Figure 5c,e) [53]. Although the Se content was higher in Santa Fé, it was more efficiently compartmentalized in 606, especially during imbibition and eophyll expansion.

Selenium, incorporated primarily into selenoproteins as selenocysteine and selenomethionine, varies widely in seeds from 0.46 to 356  $\mu\text{g}\cdot\text{g}^{-1}$ , averaging around 50  $\mu\text{g}\cdot\text{g}^{-1}$ . Genotype 606's average Se matched this range, while Santa Fé contained twice the typical amount ( $102 \pm 6.2 \mu\text{g}\cdot\text{g}^{-1}$ ). Se functions as an enzymatic cofactor, reduces oxidative stress, mitigates manganese toxicity, and supports root and aerial growth [18,19,54,55].

Selenium also exhibits a beneficial effect when applied in the form of nanoparticles, primarily used in seed nanoprimering. Recent studies have shown that this practice enhances germination due to the antioxidant effect that selenium exerts on cells, protecting them against oxidative stress, thereby improving the uniformity and rate of germination, which directly impacts seed quality and vigor [56,57].

Net accumulation change (NAC) analysis revealed that genotype 606 released more P, whereas Santa Fé showed greater Se consumption. The total activity index (TAI) indicated higher metabolic activity in 606 for releasing these macronutrients, suggesting Santa Fé achieved Se consumption with relatively lower metabolic effort.

#### 4.5. Mobilization and Metabolism of Micronutrients Reserves

The most abundant micronutrients detected in the seed samples were, in descending order, Zn, Fe, Mn, Cu, and B. Each showed particular metabolic dynamics across the evaluated stages within each of the genotypes. Regarding Se, although categorized as a micronutrient, its concentration was notably high compared to the others.

Our results show that Zn and Fe are more abundant in Santa Fé. Nonetheless, Zn consumption and release were more intensive in 606, whereas Santa Fé exhibited stronger Fe metabolism.

Zn, Fe, Mn, Cu, and B play diverse roles in germination metabolism. Zn and Fe enhance germination performance, root growth, and enzymatic function; adequate concentrations help prevent deficiencies and improve seedling vigor [58–60]. Mn and B can induce toxicity symptoms that hamper seedling development; however, appropriate B levels promote germination and vigor, and Mn activates phosphatase enzymes and lipid metabolism [54,61–64].

Boron also plays a key role in cell wall formation, membrane integrity, and supports sugar transport within the plant. Recent studies indicate that foliar application of this micronutrient can positively impact seed quality by enhancing germination capacity and improving the initial vigor of seedlings [65]. Moreover, seed treatments with boron, especially seed coatings, have been shown to induce germination and promote early seedling growth, particularly under stressful conditions [66,67]. Another important benefit of boron is its role in reducing seed-borne phytopathogen attacks, thereby contributing to improved physiological seed quality [68]. Therefore, boron mobilization is essential during the early stages of germination.

Like boron, calcium is also an important mineral for cell wall formation and additionally supports cellular signaling mechanisms in plants [65]. During early development, calcium mobilization is essential to ensure cellular integrity and proper functioning of physiological processes [65,69,70]. Recent studies indicate a synergistic effect between calcium and boron, showing that foliar application of both nutrients results in positive effects on seed production and quality [65]. Moreover, under stressful conditions, calcium enhances defense mechanisms and osmotic regulation, promoting germination and early seedling development [69]. When calcium oxide is applied in seed nanoprimering, it improves germination rates as well as increases seedling resistance to environmental stresses [70].

Mn uniquely showed significant differences in final metabolic balance (NAC), with both genotypes consuming it; 606 consumed more. Metabolic activity (TAI), however, was higher in Santa Fé, indicating that 606 mobilizes more Mn with less metabolic effort. This suggests that Mn concentration and efficient mobilization in 606 contribute to its superior germination performance, as reflected in enhanced radicle protrusion, germination percentage and germination speed compared to Santa Fé [10].

#### 4.6. Total Mobilization and Metabolism

Based on the total metabolic dynamics and intensities, the metabolic markers characterizing genotype 606 involve degradation of starch, P and Mg at the onset of germination. This genotype is also marked by the release of Ca, Se, Zn, and Cu, highlighting reserve and mineral differences during the crucial imbibition phase. In contrast, genotype Santa Fé at

this same stage exhibits markers associated with sucrose and fructose degradation, Zn and Mn mobilization, as well as lipogenesis and the release of K and S.

From radicle protrusion onwards, metabolic distinctions align with seedling development. Considering the findings of Gonçalves et al. (2024) on germination morphology, the 606 genotype's metabolism likely facilitates its reduced time taken to reach radicle protrusion [10].

During early post-germinative stages, Santa Fé shows lower metabolic rates of primary reserves but elevated mineral metabolism, likely underpinning its faster primary root elongation. Later metabolic behaviors in Santa Fé may explain its superior speed until epicotyl emergence [10].

Conversely, despite Santa Fé's early developmental advantage, higher mineral metabolic intensity in 606 during the final stage may correlate with increased expansion speed of the first pair of leaves. The principal component analysis (PCA) reveals that carbohydrates, proteins, amino acids, P and Mg cluster oppositely to lipids, Ca, Mn, B, Se, Cu, S and Zn along the PC1 axis, suggesting inverse metabolic patterns [10]. Notably, starch accumulation peaks in the secondary root stage in genotype 606. This implies that lipids are likely metabolized and converted into starch to secure energy and carbon reserves, a dynamic more intense in 606 but also present in Santa Fé, though less so. PCA component 2 separates lipid metabolites in the early Santa Fé stages. The late-stage increases in starch in both genotypes likely result from lipid conversion, supporting seedling development with expanded leaves.

Additionally, lipids and minerals—except P and Mg—are metabolically most active in initial stages, especially during the first four stages in 606, and first five in Santa Fé. Other reserves assume greater metabolic roles in later stages (from stage five onward in 606, stage six in Santa Fé).

Starch content rises in both genotypes throughout germination, but transient synthesis declines from secondary root stage in 606 and epicotyl emergence in Santa Fé, suggesting starch accumulation during late development is derived from other reserves.

The surge in sucrose synthesis in the last two stages in 606, and all carbohydrate synthesis in Santa Fé during these stages, likely relate to beta-oxidation within the glyoxylate cycle and subsequent gluconeogenesis. These pathways generate carbon sources for carbohydrate biosynthesis. Hexoses from gluconeogenesis may also participate in cell wall construction, possibly explaining the lignified embryos observed in later stages by Penfield et al. (2004) [64].

The metabolic processes observed, particularly those involving carbohydrate and lipid reserves, highlight their essential role in early seedling development as the primary sources of energy and carbon, especially in oleaginous species [71,72]. This energy demand is met through the interconversion between carbohydrates and lipids, recently elucidated in *Brassica napus*, where under water stress, plants convert lipids into carbohydrates to compensate for the energy deficit caused by stress, thereby ensuring germination and seedling growth [72,73].

This dynamic is regulated at the genetic level to balance the rapid mobilization of starch and the more gradual conversion of lipids [73,74]. Starch serves as a readily available, short-term energy reserve metabolized in the early germination stages, whereas lipids act as a long-term reserve. This gradual interconversion enhances the resistance and vigor of oleaginous plants by efficiently coordinating carbohydrate and lipid metabolism, which is crucial for successful plant establishment under stress conditions [72,73].

Such distinct metabolic traits inherent to each genotype may underlie observed differences in the germination percentages, germination speed index, mean germination velocity and developmental timings described by Gonçalves et al. (2024) [10].

## 5. Conclusions

Our findings indicate that the metabolic patterns observed during the germination of the genotypes 606 and Santa Fé of *Bertholletia excelsa* help to bridge important knowledge gaps regarding the mobilization of primary and mineral reserves in the early development of this species. The inherent differences in the amounts and metabolic activities between the two genotypes demonstrate that each adopts distinct strategies for utilizing stored resources during germination and initial growth. These results highlight that both the levels and relative concentrations of metabolites may serve as potential biochemical markers. At the same time, the specific dynamics of reserve mobilization can further provide metabolic indicators capable of distinguishing between genotypes, considering that other genetic materials have been studied in the genetic improvement programs of the Brazil nut tree.

Furthermore, we propose that future studies investigate the physiological and molecular responses of these contrasting genotypes under environmental stress conditions to identify tolerance-related biomarkers. Such integrative approaches could enhance restoration and reforestation strategies in degraded Amazonian areas, providing a solid foundation for the selection of genotypes that are more tolerant to environmental fluctuations and resilient to climate variability and habitat disturbance.

**Author Contributions:** Conceptualization, E.G., J.C. and J.F.G.; methodology, E.G., J.C., C.V., K.G., S.S., P.A. and J.F.G.; software, E.G.; validation, E.G., J.C. and J.F.G.; formal analysis, E.G., J.C., C.V., K.C., P.S., A.M., W.A. and J.C.; investigation, E.G., J.C. and J.F.G.; resources, E.G., J.C., A.M., W.A., R.L. and J.F.G.; data curation, E.G. and J.C.; writing—original draft preparation, E.G., J.C., K.C. and J.F.G.; writing—review and editing, E.G., J.C., C.V., K.C., A.F. and J.F.G.; visualization, E.G., A.M., W.A., J.C. and J.F.G.; supervision, J.C., K.C. and J.F.G.; project administration, E.G. All authors have read and agreed to the published version of the manuscript.

**Funding:** Coordination for the Improvement of Higher-Level Personnel (CAPES, Finance code 001) to E.G.; Amazonas Research Foundation (FAPEAM, POSGRAD UEA 2024-2025); National Council for Scientific and Technological Development (CNPq, 308493/2022-2 to J.F.G.).

**Data Availability Statement:** The original contributions presented in this study are included in the article material. Further inquiries can be directed to the corresponding author.

**Acknowledgments:** The authors thank the Ministério da Ciência, Tecnologia e Inovações/Instituto Nacional de Pesquisas da Amazônia (MCTI/INPA). We also want to thank the Coordenação de Aperfeiçoamento de Pessoal de Nível Superior (CAPES), Conselho Nacional de Desenvolvimento Científico e Tecnológico (CNPq, Brazil) and Fundação de Amparo à Pesquisa do Estado do Amazonas (FAPEAM). This work was funded by Coordenação de Aperfeiçoamento de Pessoal de Nível Superior—Finance code 001. Research fellowship granted by CNPq-PQ to José Francisco de Carvalho Gonçalves are also gratefully acknowledged. Finally, thanks are extended to the Postgraduate Program in Biodiversity and Biotechnology—BIONORTE Network. We sincerely thank Aruanã Agricultural Company (Itacoatiara, AM) for providing the seeds evaluated in this study and the necessary conditions for collecting the plant material.

**Conflicts of Interest:** The authors declare no conflicts of interest.

## References

1. Flores, B.M.; Montoya, E.; Sakschewski, B.; Nascimento, N.; Staal, A.; Betts, R.A.; Levis, C.; Lapola, D.M.; Esquivel-Muelbert, A.; Jakovac, C.; et al. Critical Transitions in the Amazon Forest System. *Nature* **2024**, *626*, 555–564. [\[CrossRef\]](#)
2. Souza, D.C.; Engel, V.L. Seed Functional Traits as Predictors of Seedling Establishment Success in Brazilian Tropical Forest Restoration. *Biotropica* **2024**, *56*, e13355. [\[CrossRef\]](#)
3. Faria, F.S.; Ordóñez-Parra, C.A.; Granata, L.; Resende, L.V.; Silveira, F.A.O. Low-Cost Technology Supports Propagation of Endemic Species from a Global Biodiversity Hotspot. *Restor. Ecol.* **2025**, *33*, e70005. [\[CrossRef\]](#)
4. Turchetto, F.; Araujo, M.M.; Griebeler, A.M.; Ferreira, P.A.A.; Berghetti, Á.L.P.; Aimi, S.C.; Costella, C. Intensive Silvicultural Practices Enhance the Performance of Forest Species in Restoration Plantations. *J. For. Res.* **2025**, *30*, 57–65. [\[CrossRef\]](#)



5. Zuhri, M.; Setiawan, N.N.; Dewi, S.P.; Sulistyawati, E. Seed Germination Variability and Its Association with Functional Traits in Submontane Tropical Forest Species of Indonesia: Recommendations for Direct Seeding. *For. Sci. Technol.* **2025**, *21*, 64–73. [\[CrossRef\]](#)
6. de Carvalho, J.C.; Gonçalves, J.F.d.C.; Fernandes, A.V.; da Costa, K.C.P.; de Lima e Borges, E.E.; Araújo, W.L.; Nunes-Nesi, A.; Ramos, M.V.; Rathinasabapathi, B. Reserve Mobilization and the Role of Primary Metabolites during the Germination and Initial Seedling Growth of Rubber Tree Genotypes. *Acta Physiol. Plant.* **2022**, *44*, 80. [\[CrossRef\]](#)
7. de Carvalho, J.C.; Nascimento, G.d.O.; Fernandes, A.V.; Gonçalves, E.V.; dos Santos, P.P.; Santos, A.S.; Gonçalves, J.F.d.C. Understanding the Role of Storage Reserve Mobilization during Seed Germination and Initial Seedling Growth in Species of the Genus *Carapa*. *Botany* **2024**, *102*, 268–281. [\[CrossRef\]](#)
8. Balaji, D.; Koothan, V.; Nallusamy, S.; Alagarsamy, S.; Ramalingam, S.; Ramaswamy, V. Exploring Metabolic Pathways and Phytohormonal Influence in Preharvest Sprouting Resistant and Susceptible Rice Genotypes. *Trop. Plant Biol.* **2025**, *18*, 12. [\[CrossRef\]](#)
9. da Costa, K.C.P.; de Carvalho Gonçalves, J.F.; Gonçalves, A.L.; da Rocha Nina Junior, A.; Jaquetti, R.K.; de Souza, V.F.; de Carvalho, J.C.; Fernandes, A.V.; Rodrigues, J.K.; de Oliveira Nascimento, G.; et al. Advances in Brazil Nut Tree Ecophysiology: Linking Abiotic Factors to Tree Growth and Fruit Production. *Curr. For. Rep.* **2022**, *8*, 90–110. [\[CrossRef\]](#)
10. Gonçalves, E.V.; de Carvalho, J.C.; dos Santos, P.P.; da Costa, K.C.P.; Júnior, A.d.R.N.; Alves, L.C.; Gonçalves, K.D.; de Lima, R.M.B.; Fernandes, A.V.; Araújo, W.L.; et al. Deciphering the Role of the Morphophysiology of Germination and Leaves Morphoanatomy for Differentiation of Brazil Nut Genotypes. *Rev. Bras. Bot.* **2024**, *47*, 27–45. [\[CrossRef\]](#)
11. Guimarães, Z.T.M.; de Lima Lopes, L.F.; Ferreira, M.J. Productivity and Stem Quality of Amazon Tree Species: Effects of Initial Seedling Size and Site Preparation Methods. *For. Sci.* **2025**, *71*, 1–20. [\[CrossRef\]](#)
12. de Oliveira, S.S.; Costa, K.C.P.; de Lima, R.M.; da Rocha Nina Junior, A.; de Carvalho, J.C.; Nunes-Nesi, A.; Araújo, W.L.; de Carvalho Gonçalves, J.F. *Bertholletia Excelsa* Saplings Respond to Seasonal Precipitation Variations by Changing Metabolism When Fertilized with NPK in Different Planting Systems. *For. Ecol. Manag.* **2024**, *572*, 122325. [\[CrossRef\]](#)
13. de Oliveira, I.V.; da Costa, K.C.P.; da Rocha Nina Junior, A.; de Carvalho, J.C.; de Carvalho Gonçalves, J.F. Brazil Nut Tree Increases Photosynthetic Activity and Stem Diameter Growth after Thinning. *Theor. Exp. Plant Physiol.* **2024**, *36*, 251–263. [\[CrossRef\]](#)
14. Da Costa, K.C.P.; Kirmayr Jaquetti, R.; Gonçalves, J.F.D.C. Special Issue in Honour of Prof. Reto J. Strasser—Chlorophyll a Fluorescence of *Bertholletia Excelsa* Bonpl. Plantations under Thinning, Liming, and Phosphorus Fertilization. *Photosynthetica* **2020**, *58*, 323–330. [\[CrossRef\]](#)
15. Passos, R.M.D.O.; Celso, P.; De, P.; Roberval, A.; Bezerra De Lima, M.; Rodrigues De Souza, C. *Características Biométricas e Produção de Frutos de Castanha-Da-Amazônia Em Plantios Clonais Na Amazônia Central*; Embrapa: Brasília, Brazil, 2008.
16. de Camargo, I.P.; Mauro de Castro, E.; Losada Gavilanes, M. Aspectos da anatomia e morfologia de amêndoas e plântulas de castanheira-do-brasil. *Cerne* **2000**, *6*, 11–18.
17. Gonçalves, J.F.d.C.; Fernandes, A.V.; Fernando Oliveira, A.M.; Rodrigues, L.F.; Marengo, R.A. Seed components of amazon trees primary metabolism components of seeds from Brazilian Amazon tree species. *Braz. J. Plant Physiol.* **2002**, *14*, 139–142. [\[CrossRef\]](#)
18. Lima, L.W.; Stonehouse, G.C.; Walters, C.; El Mehdawi, A.F.; Fakra, S.C.; Pilon-Smits, E.A.H. Selenium Accumulation, Speciation and Localization in Brazil Nuts (*Bertholletia Excelsa* H.B.K.). *Plants* **2019**, *8*, 289. [\[CrossRef\]](#)
19. Junior, E.C.d.S.; Duran, N.M.; de Lima Lessa, J.H.; Ribeiro, P.G.; de Oliveira Wadt, L.H.; da Silva, K.E.; de Lima, R.M.B.; Batista, K.D.; Guedes, M.C.; de Oliveira, R.C.; et al. Unraveling the Accumulation and Localization of Selenium and Barium in Brazil Nuts Using Spectroanalytical Techniques. *J. Food Compos. Anal.* **2022**, *106*, 104329. [\[CrossRef\]](#)
20. El-Maarouf-Bouteau, H. The Seed and the Metabolism Regulation. *Biology* **2022**, *11*, 168. [\[CrossRef\]](#)
21. Shukla, R.; Kumar, A.; Prasad, C.S.; Srivastava, B.; Dubey, N.K. Antimycotic and Antiaflatoxigenic Potency of *Adenocalymma Alliaceum* Miers. on Fungi Causing Biodeterioration of Food Commodities and Raw Herbal Drugs. *Int. Biodeterior. Biodegrad.* **2008**, *62*, 348–351. [\[CrossRef\]](#)
22. Jisieike, C.F.; Betiku, E. Rubber Seed Oil Extraction: Effects of Solvent Polarity, Extraction Time and Solid-Solvent Ratio on Its Yield and Quality. *Biocatal. Agric. Biotechnol.* **2020**, *24*, 101522. [\[CrossRef\]](#)
23. Fernie, A.R.; Roscher, A.; Ratcliffe, R.G.; Kruger, N.J. Fructose 2,6-Bisphosphate Activates Pyrophosphate: Fructose-6-Phosphate 1-Phosphotransferase and Increases Triose Phosphate to Hexose Phosphate Cycling in Heterotrophic Cells. *Planta* **2001**, *212*, 250–263. [\[CrossRef\]](#) [\[PubMed\]](#)
24. Bradford, M.M. A Rapid and Sensitive Method for the Quantitation of Microgram Quantities of Protein Utilizing the Principle of Protein-Dye Binding. *Anal. Biochem.* **1976**, *72*, 248–254. [\[CrossRef\]](#)
25. Yemm, E.W.; Cocking, E.C.; Ricketts, R.E. The Determination of Amino-Acids with Ninhydrin. *Analyst* **1955**, *80*, 209–214. [\[CrossRef\]](#)
26. dos Banhos, E.F.; Albuquerque, P.M.; Oliveira, R.L.e.; de Loiola, S.K.S.; Silva, S.N.e.; Batista, C.E.; Neta, A.S.C.; Cavalcante, L.F.Q.; Duvoisin, S., Jr. Spatial and Temporal Distribution of Potentially Toxic Elements in the Urban Area of São Raimundo Basin in Manaus, Brazil. *Rev. Ambiente Água* **2025**, *20*, e3036. [\[CrossRef\]](#)

27. Hou, X.; Jones, B.T. Inductively Coupled Plasma/Optical Emission Spectrometry. In *Encyclopedia of Analytical Chemistry*; John Wiley & Sons, Ltd.: Hoboken, NJ, USA, 2006; ISBN 9780470027318.
28. Poorter, H.; Garnier, E. Plant Growth Analysis: An Evaluation of Experimental Design and Computational Methods. *J. Exp. Bot.* **1996**, *47*, 1343–1351. [[CrossRef](#)]
29. Hunt, R. Growth Analysis, Individual Plants. In *Encyclopedia of Applied Plant Sciences*, 2nd ed.; Thomas, B., Murray, B.G., Murphy, D.J., Eds.; Academic Press: Oxford, UK, 2017; pp. 421–429, ISBN 978-0-12-394808-3.
30. Yeo, I.; Johnson, R.A. A New Family of Power Transformations to Improve Normality or Symmetry. *Biometrika* **2000**, *87*, 954–959. [[CrossRef](#)]
31. R Core Team. *R: A Language and Environment for Statistical Computing*; version 4.4.3; R Core Team: Vienna, Austria, 2025.
32. Hammer, Ø.; Harper, D.A.T.; Ryan, P.D. Past: Paleontological statistics software package for education and data analysis. *Palaeontol. Electron.* **2001**, *4*, 1–9.
33. Shaik, S.S.; Carciofi, M.; Martens, H.J.; Hebelstrup, K.H.; Blennow, A. Starch Bioengineering Affects Cereal Grain Germination and Seedling Establishment. *J. Exp. Bot.* **2014**, *65*, 2257–2270. [[CrossRef](#)]
34. Punia, A.; Kumari, M.; Chouhan, M.; Saini, V.; Joshi, R.; Kumar, A.; Kumar, R. Proteomic and Metabolomic Insights into Seed Germination of *Ferula Assa-Foetida*. *J. Proteom.* **2024**, *300*, 105176. [[CrossRef](#)]
35. MacNeill, G.J.; Mehrpouyan, S.; Minow, M.A.A.; Patterson, J.A.; Tetlow, I.J.; Emes, M.J. Starch as a Source, Starch as a Sink: The Bifunctional Role of Starch in Carbon Allocation. *J. Exp. Bot.* **2017**, *68*, 4433–4453. [[CrossRef](#)] [[PubMed](#)]
36. Smith, A.M.; Stitt, M. Coordination of Carbon Supply and Plant Growth. *Plant Cell Environ.* **2007**, *30*, 1126–1149. [[CrossRef](#)]
37. Geigenberger, P. Regulation of Sucrose to Starch Conversion in Growing Potato Tubers. *J. Exp. Bot.* **2003**, *54*, 457–465. [[CrossRef](#)]
38. Hamade, S.; Traver, M.S.; Bartel, B. The Atypical Pectin Methylesterase Family Member PME31 Promotes Seedling Lipid Droplet Utilization. *Plant Direct* **2025**, *9*, e70054. [[CrossRef](#)]
39. Wang, L.; Zheng, L.; Hu, H.; Qin, L.; Liu, H.; Wu, R.; Ren, Z.; Fu, J.; Xu, H.; Guo, H.; et al. MALDI Imaging Unveils Spatial Lipidomics Dynamics during Jojoba Seed Germination and Post-Germination. *Ind. Crops Prod.* **2024**, *220*, e70054. [[CrossRef](#)]
40. Yi, K.; Gao, L.Y.; Xu, Y.; Yang, J.; Mao, P.; Dou, L.; Li, M. Lipid Remodeling and Response Mechanisms during the Germination of Aged Oat Seeds. *BMC Plant Biol.* **2025**, *25*, 186. [[CrossRef](#)]
41. Yu, L.; Zhou, C.; Fan, J.; Shanklin, J.; Xu, C. Mechanisms and Functions of Membrane Lipid Remodeling in Plants. *Plant J.* **2021**, *107*, 37–53. [[CrossRef](#)]
42. Lopes, L.d.S.; Gallão, M.I.; Cândida, E.; Campos, H.; Bertini, M. Mobilisation of Reserves during Germination of *Jatropha* Seeds 1 Mobilização de Reservas Durante a Germinação de Sementes de Pinhão Manso. *Rev. Ciência Agronômica* **2013**, *44*, 371–378. [[CrossRef](#)]
43. Escudero-Feliu, J.; Lima-Cabello, E.; Rodríguez de Haro, E.; Morales-Santana, S.; Jimenez-Lopez, J.C. Functional Association between Storage Protein Mobilization and Redox Signaling in Narrow-Leafed Lupin (*Lupinus angustifolius* L.) Seed Germination and Seedling Development. *Genes* **2023**, *14*, 1889. [[CrossRef](#)]
44. Bewley, J.D.; Bradford, K.J.; Hilhorst, H.W.M.; Nonogaki, H. *Seeds*; Springer: New York, NY, USA, 2013; ISBN 978-1-4614-4692-7.
45. Rosental, L.; Nonogaki, H.; Fait, A. Activation and Regulation of Primary Metabolism during Seed Germination. *Seed Sci. Res.* **2014**, *24*, 1–15. [[CrossRef](#)]
46. Galili, G.; Avin-Wittenberg, T.; Angelovici, R.; Fernie, A.R. The Role of Photosynthesis and Amino Acid Metabolism in the Energy Status during Seed Development. *Front. Plant Sci.* **2014**, *5*, 447. [[CrossRef](#)]
47. Hildebrandt, T.M.; Nunes Nesi, A.; Araújo, W.L.; Braun, H.P. Amino Acid Catabolism in Plants. *Mol. Plant* **2015**, *8*, 1563–1579. [[CrossRef](#)] [[PubMed](#)]
48. Marschner, P. *Marschner's Mineral Nutrition of Higher Plants*; Elsevier: Amsterdam, The Netherlands, 2012; ISBN 9780123849052.
49. Maathuis, F.J. Physiological Functions of Mineral Macronutrients. *Curr. Opin. Plant Biol.* **2009**, *12*, 250–258. [[CrossRef](#)] [[PubMed](#)]
50. Kumar, A.; Dash, G.K.; Sahoo, S.K.; Lal, M.K.; Sahoo, U.; Sah, R.P.; Ngangkham, U.; Kumar, S.; Baig, M.J.; Sharma, S.; et al. Phytic Acid: A Reservoir of Phosphorus in Seeds Plays a Dynamic Role in Plant and Animal Metabolism. *Phytochem. Rev.* **2023**, *22*, 1281–1304. [[CrossRef](#)]
51. White, P.J.; Karley, A.J. Potassium. In *Cell Biology of Metals and Nutrients*; Springer: Berlin/Heidelberg, Germany, 2010; pp. 199–224.
52. Ahmad, I.; Maathuis, F.J.M. Cellular and Tissue Distribution of Potassium: Physiological Relevance, Mechanisms and Regulation. *J. Plant Physiol.* **2014**, *171*, 708–714. [[CrossRef](#)]
53. Eggert, K.; von Wirén, N. Dynamics and Partitioning of the Ionome in Seeds and Germinating Seedlings of Winter Oilseed Rape. *Metallomics* **2013**, *5*, 1316–1325. [[CrossRef](#)]
54. Sieprawska, A.; Skórka, M.; Bednarska-Kozakiewicz, E.; Niedojadło, K.; Janiak, A.; Telk, A.; Filek, M. Significance of Selenium Supplementation in Root- Shoot Reactions Under Manganese Stress in Wheat Seedlings—Biochemical and Cytological Studies. *Plant Soil* **2021**, *468*, 389–410. [[CrossRef](#)]

55. Awasthi, S.; Chauhan, R.; Srivastava, S. Chapter 2—The Importance of Beneficial and Essential Trace and Ultratrace Elements in Plant Nutrition, Growth, and Stress Tolerance. In *Plant Nutrition and Food Security in the Era of Climate Change*; Kumar, V., Srivastava, A.K., Suprasanna, P., Eds.; Academic Press: Cambridge, MA, USA, 2022; pp. 27–46, ISBN 978-0-12-822916-3.
56. García-Locascio, E.; Valenzuela, E.I.; Cervantes-Avilés, P. Impact of Seed Priming with Selenium Nanoparticles on Germination and Seedlings Growth of Tomato. *Sci. Rep.* **2024**, *14*, 6726. [[CrossRef](#)] [[PubMed](#)]
57. Setty, J.; Samant, S.B.; Yadav, M.K.; Manjubala, M.; Pandurangam, V. Beneficial Effects of Bio-Fabricated Selenium Nanoparticles as Seed Nanoprimer Agent on Seed Germination in Rice (*Oryza sativa* L.). *Sci. Rep.* **2023**, *13*, 22349. [[CrossRef](#)]
58. Czarnek, K.; Tatarczak-Michalewska, M.; Dreher, P.; Rajput, V.D.; Wójcik, G.; Gierut-Kot, A.; Szopa, A.; Blicharska, E. UV-C Seed Surface Sterilization and Fe, Zn, Mg, Cr Biofortification of Wheat Sprouts as an Effective Strategy of Bioelement Supplementation. *Int. J. Mol. Sci.* **2023**, *24*, 10367. [[CrossRef](#)]
59. Neverov, A.A. Stimulating Role of Trace Elements at the Stage of Germination of Barley Seeds. *Anim. Husb. Fodd. Prod.* **2022**, *105*, 159–170. [[CrossRef](#)]
60. Kaur, H.; Gupta, N.; Kaur Gill, G. Sole and Combined Effect of Micronutrients on Germination and Seedling Growth Attributes of Sweet Corn (*Zea mays* L. Saccharata). *J. Plant Nutr.* **2023**, *46*, 2473–2487. [[CrossRef](#)]
61. Khan, A.; Bibi, S.; Javed, T.; Mahmood, A.; Mehmood, S.; Javaid, M.M.; Ali, B.; Yasin, M.; Abidin, Z.U.; Al-Sadoon, M.K.; et al. Effect of Salinity Stress and Surfactant Treatment with Zinc and Boron on Morpho-Physiological and Biochemical Indices of Fenugreek (*Trigonella Foenum-Graecum*). *BMC Plant Biol.* **2024**, *24*, 138. [[CrossRef](#)]
62. Bessa, L.A.; Vitorino, L.C.; Silva, F.G. Micronutrient Deficiency Affects the Development of the Seedlings of the Cagaita, a Myrtaceae Typical of the Brazilian Cerrado. *Res. Soc. Dev.* **2020**, *9*, e65391110209. [[CrossRef](#)]
63. Campbell, L.C.; Nable, R.O. *Physiological Functions of Manganese in Plants*; Springer: Berlin/Heidelberg, Germany, 1988.
64. Penfield, S.; Rylott, E.L.; Gilday, A.D.; Graham, S.; Larson, T.R.; Graham, I.A. Reserve Mobilization in the Arabidopsis Endosperm Fuels Hypocotyl Elongation in the Dark, Is Independent of Abscissic Acid, and Requires Phosphoenolpyruvate Carboxykinase1. *Plant Cell* **2004**, *16*, 2705–2718. [[CrossRef](#)]
65. Cardoso, A.I.I.; Colombari, L.F.; Silva, G.F.; Chaves, P.P.N.; Nogueira, B.B.; Putti, F.F. Calcium and Boron Foliar Application in the Production and Quality of Sweet Pepper Seeds. *Hortic. Bras.* **2022**, *40*, 373–377. [[CrossRef](#)]
66. Kumar, T.; Tama, P.M.; Kabir Hemel, S.A.; Ghosh, R.K.; Ali, M.I.; Al-Bakky, A.; Alim, A. Optimizing Boron Application Methods and Dosages to Enhance Jute (*Corchorus Olitorius*) Seed Yield and Quality under Sub-Tropical Climate. *Heliyon* **2025**, *11*, e42320. [[CrossRef](#)] [[PubMed](#)]
67. Dos Santos Cordeiro, C.F.; Galdi, L.V.; Silva, G.R.A.; Custodio, C.C.; Echer, F.R. Boron Nutrition Improves Peanuts Yield and Seed Quality in a Low B Sandy Soil. *Rev. Bras. Cienc. Solo* **2024**, *48*, e0230043. [[CrossRef](#)]
68. Kaya, M.D.; Ergin, N. Boron Seed Treatments Induce Germination and Seedling Growth by Reducing Seed-Borne Pathogens in Safflower (*Carthamus tinctorius* L.). *J. Plant Prot. Res.* **2023**, *63*, 481–487. [[CrossRef](#)]
69. Mulaudzi, T.; Hendricks, K.; Mabiya, T.; Muthevuli, M.; Ajayi, R.F.; Mayedwa, N.; Gehring, C.; Iwuoha, E. Calcium Improves Germination and Growth of Sorghum Bicolor Seedlings under Salt Stress. *Plants* **2020**, *9*, 730. [[CrossRef](#)]
70. Mazhar, M.W.; Ishtiaq, M.; Maqbool, M.; Akram, R. Seed Priming with Calcium Oxide Nanoparticles Improves Germination, Biomass, Antioxidant Defence and Yield Traits of Canola Plants under Drought Stress. *S. Afr. J. Bot.* **2022**, *151*, 889–899. [[CrossRef](#)]
71. Zhu, M.; Zang, Y.; Zhang, X.; Shang, S.; Xue, S.; Chen, J.; Tang, X. Insights into the Regulation of Energy Metabolism during the Seed-to-Seedling Transition in Marine Angiosperm *Zostera marina* L.: Integrated Metabolomic and Transcriptomic Analysis. *Front. Plant Sci.* **2023**, *14*, 1130292. [[CrossRef](#)] [[PubMed](#)]
72. Sturme, M.H.J.; Gong, Y.; Heinrich, J.M.; Klok, A.J.; Eggink, G.; Wang, D.; Xu, J.; Wijffels, R.H. Transcriptome Analysis Reveals the Genetic Foundation for the Dynamics of Starch and Lipid Production in *Ettlia Oleoabundans*. *Algal Res.* **2018**, *33*, 142–155. [[CrossRef](#)]
73. Yang, H.; Bai, C.; Ai, X.; Yu, H.; Xu, Z.; Wang, J.; Kuai, J.; Zhao, J.; Wang, B.; Zhou, G. Conversion of Lipids into Carbohydrates Rescues Energy Insufficiency in Rapeseed Germination under Waterlogging Stress. *Physiol. Plant* **2024**, *176*, e14576. [[CrossRef](#)] [[PubMed](#)]
74. Chapman, K.D.; Dyer, J.M.; Mullen, R.T. Biogenesis and Functions of Lipid Droplets in Plants: Thematic Review Series: Lipid Droplet Synthesis and Metabolism: From Yeast to Man. *J. Lipid Res.* **2012**, *53*, 215–226. [[CrossRef](#)]

**Disclaimer/Publisher’s Note:** The statements, opinions and data contained in all publications are solely those of the individual author(s) and contributor(s) and not of MDPI and/or the editor(s). MDPI and/or the editor(s) disclaim responsibility for any injury to people or property resulting from any ideas, methods, instructions or products referred to in the content.